Combined U-corrected Pb-Pb dating and Al-26-Mg-26 systematics of individual chondrules - Evidence for a reduced initial abundance of Al-26 amongst inner Solar System chondrules

Bollard, Jean; Kawasaki, Noriyuki; Sakamoto, Naoya; Olsen, Mia; Itoh, Shoichi; Larsen, Kirsten; Wielandt, Daniel; Schiller, Martin; Connelly, James N.; Yurimoto, Hisayoshi; Bizzarro, Martin

Published in:
Geochimica et Cosmochimica Acta

DOI:
10.1016/j.gca.2019.06.025

Publication date:
2019

Document version
Publisher's PDF, also known as Version of record

Available online at www.sciencedirect.com

ScienceDirect

Geochimica et Cosmochimica Acta 260 (2019) 62–83

Geochimica et Cosmochimica Acta

www.elsevier.com/locate/gca

Combined U-corrected Pb-Pb dating and ^{26}Al-^{26}Mg systematics of individual chondrules – Evidence for a reduced initial abundance of ^{26}Al amongst inner Solar System chondrules

Jean Bollard [a], Noriyuki Kawasaki [b], Naoya Sakamoto [c], Mia Olsen [a], Shoichi Itoh [d], Kirsten Larsen [a], Daniel Wielandt [a], Martin Schiller [a], James N. Connelly [a] Hisayoshi Yurimoto [b,e], Martin Bizzarro [a,*]

[a] *Centre for Star and Planet Formation, Natural History Museum of Denmark, University of Copenhagen, Copenhagen DK-1350, Denmark*
[b] *Department of Natural History Sciences, Hokkaido University, Sapporo 060-0810, Japan*
[c] *Isotope Imaging Laboratory, Creative Research Institution, Hokkaido University, Sapporo 001-0021, Japan*
[d] *Department of Earth and Planetary Sciences, Kyoto University, Kyoto 606-8502, Japan*
[e] *ISAS/JAXA, Sagamihara, Kanagawa 252-5210, Japan*

Received 16 November 2018; accepted in revised form 17 June 2019; available online 22 June 2019

Abstract

Chondrites are fragments of asteroids that avoided melting and, thus, provide a record of the material that accreted to form protoplanets. The dominant constituent of chondrites are millimeter-sized chondrules formed by transient heating events in the protoplanetary disk. Some chondritic components, including chondrules, contain evidence of the extinct short-lived radionuclide ^{26}Al (half-life of 0.73 Myr). The decay of ^{26}Al is postulated to have been an important heat source promoting asteroidal melting and differentiation. Thus, understanding the ^{26}Al inventory in the accretion regions of differentiated asteroids is critical to constrain the accretion timescales of protoplanets. The current paradigm asserts that the canonical ^{26}Al/^{27}Al ratio of $\sim 5 \times 10^{-5}$ recorded by the oldest dated solids, calcium-aluminium refractory inclusions, represents that of the bulk Solar System. We report, for the first time, the ^{26}Al-^{26}Mg systematics of chondrules from the North West Africa (NWA) 5697 L 3.10 ordinary chondrite and Allende CV3$_{OxA}$ (Vigarano type) carbonaceous chondrite that have been previously dated by U-corrected Pb-Pb dating. Eight chondrules, which record absolute ages ranging from 4567.57 ± 0.56 to 4565.84 ± 0.72 Ma, define statistically-significant internal isochron relationships corresponding to initial (^{26}Al/^{27}Al) ($[^{26}Al/^{27}Al]_0$) ratios in their precursors at the time of CAI formation at 4567.3 ± 0.16 Ma ranging from $(3.92^{-2.95}_{+4.53}) \times 10^{-6}$ to $(2.74^{-1.09}_{+1.30}) \times 10^{-5}$. These initial ratios are much lower than those predicted by the Pb-Pb ages, corresponding to age mismatches between the Pb-Pb and ^{26}Al-^{26}Mg systems ranging from $0.69^{-0.44}_{+0.54}$ to $2.71^{-0.59}_{+0.66}$ Myr. All chondrules record ^{54}Cr/^{52}Cr compositions indicating an origin from inner Solar System precursor material and, as such, we interpret the age mismatch to reflect a reduced initial abundance of ^{26}Al in the chondrule precursors, similar to that proposed for the angrite parent body. In particular, the range of $[^{26}Al/^{27}Al]_0$ ratios essentially defines two groups, which are apparently correlated with the absolute ages of the chondrules. A first group, charactertized by chondrules with absolute Pb-Pb ages identical to CAIs, defines a mean $[^{26}Al/^{27}Al]_0$ value of $(4.75^{-1.21}_{+1.99}) \times 10^{-6}$, whereas a second group, with absolute ages ~1 Myr younger than CAIs, record a mean mean $[^{26}Al/^{27}Al]_0$ of $(1.82^{-0.40}_{+0.57}) \times 10^{-5}$. We interpret this systematic variability in $[^{26}Al/^{27}Al]_0$ values as reflecting progressive inward transport and admixing of dust of solar composition and ^{26}Al content from the outer disk during chondrule recycling and remelting. Finally, a reduced $[^{26}Al/^{27}Al]_0$ ratio in chondrule precursors impacts our understanding of the accretion timescales of differentiated planetesimals if chondrules are indeed representative of inner disk material. Using the average $[^{26}Al/^{27}Al]_0$

* Corresponding author.
E-mail address: bizzarro@snm.ku.dk (M. Bizzarro).

https://doi.org/10.1016/j.gca.2019.06.025
0016-7037/

ratio of $(1.36 \pm 0.72) \times 10^{-5}$ defined by the eight chondrules, thermal modelling constrains the accretion of differentiated planetesimals formed with this ^{26}Al inventory from ~0.1 to ~0.9 Myr after Solar System formation to ensure melting by ^{26}Al decay.

Keywords: Solar System; Chondrites; Chondrules; 26Al distribution; Absolute age dating; Asteroid accretion

1. INTRODUCTION

Meteorites and their components provide a record of the processes associated with the formation of the Solar System, from the collapse of the protosolar molecular cloud through the formation and earliest evolution of the protoplanetary disk (Krot et al., 2009). The accretion of disk solids to form rocky bodies of chondritic composition, and their subsequent differentiation into asteroids consisting of a metallic core, peridotitic mantle, and basaltic crust, represents the first steps leading to the formation of terrestrial planets. Simulations of evolving disks suggest that the accretion of pebbles into km-sized planetesimals is a rapid and efficient process (Johansen et al., 2015). Early accretion in the young Solar System results in the incorporation of heat-generating short-lived radioisotopes such as ^{26}Al (^{26}Al decays to ^{26}Mg with a half-life of 0.73 Myr) resulting in wide-scale melting, differentiation and extensive volcanic activity (Urey, 1955; Lee et al., 1976; Bizzarro et al., 2005; Hevey and Sanders, 2006). As such, the accretion timescales of differentiated planetesimals are highly dependent on the available heat budget, namely the abundance of ^{26}Al at the time of accretion. Constraining the onset of planetesimal accretion and, by extension, the emergence of protoplanets during the evolution of the protoplanetary disk is central to testing models of planet formation.

It is commonly assumed that the stellar-derived short-lived radionuclide ^{26}Al was injected into the nascent Solar System (i.e. Gaidos et al., 2009; Ouelette et al., 2009; Vasileiadis et al., 2013) and homogenized amongst Solar System solids during the earliest evolution of the solar protoplanetary disk. In this model, the initial canonical ^{26}Al/^{27}Al ratio of $\sim 5 \times 10^{-5}$ (Jacobsen et al., 2008; Larsen et al., 2011) recorded by the oldest disk solids, calcium-aluminum-rich inclusions (CAIs), is believed to represent the initial abundance of ^{26}Al for the Solar System as a whole. This simplistic view, however, has been recently challenged by a number of studies. For example, the contemporaneous formation of refractory inclusions with contrasting initial abundances of ^{26}Al suggest that this nuclide may have been spatially or temporally heterogeneously distributed in the CAI-forming region (Thrane et al., 2008; Makide et al., 2011; Holst et al., 2013). Therefore, the apparently restricted range of inferred initial ^{26}Al/^{27}Al ratios defined by bulk analyses of CAIs from CV (Vigarano type) carbonaceous chondrites (Jacobsen et al., 2008; Larsen et al., 2011) does not necessarily imply a homogeneous distribution of ^{26}Al throughout the solar proto-planetary disk during and after the epoch of CAI formation. Moreover, Larsen et al. (2011) reported heterogeneity in the mass-independent ^{26}Mg composition (^{26}Mg*) of bulk Solar System reservoirs with solar or near-Solar Al/Mg ratios interpreted as reflecting variability in the initial abundance of ^{26}Al, perhaps up to 80% of the canonical value. Similarly, van Kooten et al. (2016) recently suggested based on Mg and Cr isotopes that metal-rich chondrites and their components accreted in an ^{26}Al-poor reservoir located beyond the orbits of the gas giants. Chronometers based on short-lived radionuclides, such as ^{26}Al, rely on the assumption of initial homogeneous distribution of the parent radionuclide throughout the protoplanetary disk. Variability in the ^{26}Al distribution, as suggested by the observed ^{26}Mg* heterogeneity, would invalidate ages based on the Al-Mg systematics in Solar System objects except in cases where samples were derived from a common source. Consequently, these studies call for a critical reassessment of the assumption of Solar System ^{26}Al homogeneity.

The only robust method to assess the degree of ^{26}Al homogeneity in the solar protoplanetary disk requires comparison with the U-corrected Pb-Pb chronometer using samples with simple thermal histories. Unlike ages derived from short-lived radioisotope chronometers, U-corrected Pb-Pb ages are free from the assumption of parent nuclides homogeneity. Such an approach, first initiated by Nyquist et al. (2009) but with Pb-Pb ages that were not corrected for U isotope variations, was successfully conducted by Schiller et al. (2015a) on three magmatic meteorites. Indeed, rapidly-cooled magmatic meteorites such as angrites are typically targeted for such comparisons, given that the amount of sample available is large enough to obtain both high-resolution ^{26}Al-^{26}Mg and uranium-corrected Pb-Pb ages. Using their U-corrected absolute Pb-Pb ages as reference, their Al-Mg ages indicate a reduced initial ^{26}Al/^{27}Al value by a factor ~4 in the accretion region of the angrite parent body compared to the canonical value, which supports the view of ^{26}Al heterogeneity (Schiller et al., 2015a).

To further explore the significance of the apparent reduced initial ^{26}Al/^{27}Al value in angrites, we extend our analysis to chondrules, the most abundant chondritic component. Chondrules are millimeter-sized silicate-rich spherule-like objects comprising up to 80% by volume of chondrite meteorites (Jones, 1990; Scott, 2007). The majority of chondrules are believed to have formed as dust aggregates of near-solar composition that are subsequently melted by a flash heating mechanism and rapidly cooled (Zanda 2004). As such, chondrules may provide a robust means of investigating the level of consistency between the ^{26}Al-^{26}Mg and Pb-Pb systems given the simple cooling histories of these objects. Importantly, it is now established that chondrule formation began contemporaneously with CAIs and lasted at least ~4 Myr, occurring in different regions of the protoplanetary disk (Connelly et al. 2012;

Bollard et al. 2017). Moreover, given their sheer abundance in chondrite meteorites, chondrules are thought to dominate the precursor material of differentiated planetesimals and, by extension, of planetary bodies. Therefore, these objects allow us to probe the inventory of ^{26}Al in the precursor material of protoplanets during the entire disk lifetime. In this paper, we report on the ^{26}Al-^{26}Mg systematics of eight chondrules previously dated by the U-corrected Pb-Pb method (Connelly et al. 2012; Bollard et al. 2017). The initial ^{26}Al/^{27}Al ratios are defined by the internal mineral isochron approach using in situ methods. These data are complemented by oxygen-isotope measurements of the various phases used for isochron relationships as well as bulk Mg and ^{54}Cr isotope compositions of individual chondrules. Finally, we examine the consequences of potential initial ^{26}Al variability in disk material such as chondrules on heating timescales and extent of asteroid differentiation using thermal modeling

2. MATERIAL AND METHODS

To probe the inventory of ^{26}Al in chondrule-forming regions, we defined the initial ^{26}Al/^{27}Al ratios of eight chondrules with known absolute ages (Connelly et al. 2012; Bollard et al., 2017) through the internal ^{26}Al-^{26}Mg isochron approach by combining measurements obtained by secondary ionization mass spectrometry (SIMS) and high-resolution inductively coupled plasma source mass spectrometry (HR-MC-ICPMS). The chondrules were primarily selected for Pb-Pb dating, such that the requirements for precise and accurate ^{26}Al-^{26}Mg dating were not prioritized at the outset. Our sample suite includes one CV3 Allende chondrule (C30) with a U-corrected Pb-Pb age of 4567.32 ± 0.42 Myr (all uncertainties are quoted at 95% confidence level) as well as seven chondrules from the ordinary chondrite L3.10 NWA 5697: 2-C1 (4567.57 ± 0.56 Myr), 5-C2 (4567.54 ± 0.52 Myr), 5-C10 (4567.41 ± 0.57 Myr) C1 (4566.67 ± 0.43 Myr), 3-C5 (4566.20 ± 0.63 Myr), C3 (4566.02 ± 0.26 Myr), and 11-C1 (4565.84 ± 0.72 Myr) (Table 1 and 2). The petrology and mineral chemistry of the chondrules investigated in this work are published in full elsewhere (Connelly et al., 2012; Bollard et al., 2017) and are summarized in Table 1. The existence of oxygen isotope variations amongst individual chondrules (Chaussidon et al., 2008; Kita et al., 2010) suggests that some minerals may not be comagmatic and, thus, care must be taken in the interpretation of Al-Mg isochron relationships in these cases. Thus, we have determined the oxygen-isotope compositions of the minerals studied for their ^{26}Al-^{26}Mg systematics and these are reported in Table 3.

2.1. In situ Al-Mg and O isotope measurements

The internal ^{26}Al-^{26}Mg systematics and oxygen isotope compositions of minerals in chondrules were measured by secondary ion mass spectrometry (SIMS, Cameca IMS-1280HR) at Hokkaido University, with the full analytical procedures reported in Kawasaki et al. (2017, 2018). Polished sections were coated with a gold thin film (~70 nm) for the SIMS measurements. An $^{16}O^-$ primary beam accelerated to 23 keV was employed for Al-Mg isotopic measurements. We used both peak-jumping mode and multicollection mode, depending on the secondary ion intensities of magnesium isotopes from the minerals. For Mg-rich phases (olivine and spinel), the Mg isotopes ($^{24}Mg^{\pm}$, $^{25}Mg^{\pm}$, and $^{26}Mg^{\pm}$) and $^{27}Al^{\pm}$ were measured simultaneously in the multicollection mode with four Faraday cups. The primary beam current was set to 7 nA with a size of ~15 μm for the olivine measurements, whereas a 6–8 nA current with beam size of ~10–15 μm was used for spinel measurements depending on the spinel chemical compositions. The mass resolution of M/ΔM was set at ~2000. The contributions of ion interferences (e.g., $^{48}Ca^{2+}$, $^{24}MgH^{\pm}$, $^{25}MgH^{\pm}$, and $^{52}Cr^{2+}$) were negligible under these conditions. The secondary ion intensities of $^{24}Mg^{\pm}$ were ~5×10^8 cps and ~$0.4–2.0 \times 10^8$ cps olivine and spinel, respectively. Each measurement was conducted in 20 cycles with 10 s counting time per cycle. For Al-rich phases (plagioclase and mesostasis), magnesium isotopes ($^{24}Mg^{\pm}$, $^{25}Mg^{\pm}$, and $^{26}Mg^{\pm}$) were measured using an electron multiplier in monocollection mode, whereas $^{27}Al^{\pm}$ was measured using a Faraday cup with the peak jumping mode of a sector magnet. The primary beam current was set to 0.2–0.8 nA with a size of ~5–10 μm, adjusted for each analysis according to variations of chemical compositions to obtain sufficient secondary ion intensities. The mass resolution (M/ΔM) of the instrument was set at ~3500, which is sufficient to resolve Mg hydride interferences at masses 25 and 26. The secondary ion intensities of $^{24}Mg^{\pm}$ were typically ~2×10^5 cps. Each measurement was conducted for 50 cycles with a counting sequence of $^{24}Mg^{\pm}$ for 3 s,

Table 1
Petrology and mineralogy of the eight chondrules investigated.

Meteorite	Class	Chondrule	Type	Texture	Minerals
NWA 5697	L3.10	2-C1	IA	BO	Ol, Px, Cpx, An-Mes
NWA 5697	L3.10	5-C2	IIAB	BOP	Ol, Px, Cpx, An-Mes
NWA 5697	L3.10	5-C10	IIAB	BOP/SOP	Ol, Px, Cpx, An-Mes, Cr-Sp
Allende	CV3	C30	IIAB	MP	Ol, Px, Cpx, An-Mes, Cr-Sp
NWA 5697	L3.10	C1	IA	BO	Ol, Px, Cpx, An-rich Mes
NWA 5697	L3.10	3-C5	IIAB	POP	Ol, Px, Cpx, An-Mes, Cr-Sp
NWA 5697	L3.10	C3	IIAB	FG	Ol, Px, Cpx, Mes
NWA 5697	L3.10	11-C1	IIAB	BOP	Ol, Px, Cpx, An-Mes, Cr-Sp

Notes: BO, barred olivine, BOP, barred olivine-pyroxene, SOP, skeletal olivine-pyroxene, MP, microporphyritic, POP, porphyritic olivine-pyroxene, FG, fine-grained. Ol, olivine, Px, low-Ca pyroxene, Cpx, high-Ca clinopyroxene, An-Mes, Anorthic mesostasis, Cr-Sp, Cr-spinel.

Table 2
Summary of Pb-Pb ages, $^{238}U/^{235}U$ ratios used in age calculation, ^{54}Cr compositions, and Al-Mg systematics of the eight individual chondrules investigated.

Meteorite	Chondrule	Age (Myr)	$^{238}U/^{235}U$	$\mu^{54}Cr$ (ppm)	$(^{26}Al/^{27}Al)_{TC} \times 10^{-6}$	$[^{26}Al/^{27}Al]_0$	$\mu^{26}Mg_0$ (ppm)	Age offset (Myr)
NWA 5697	2-C1*	4567.57 ± 0.56	137.779 ± 0.022	−40 ± 18	7.56 ± 1.53	$(5.85^{-2.66}_{+4.43}) \times 10^{-6}$	−11.8 ± 1.3	$2.31^{-0.61}_{+0.63}$
NWA 5697	5-C2*	4567.54 ± 0.52	137.756 ± 0.029	7 ± 15	7.04 ± 1.51	$(5.62^{-2.48}_{+4.02}) \times 10^{-6}$	−8.6 ± 2.9	$2.35^{-0.59}_{+0.61}$
NWA 5697	5-C10	4567.41 ± 0.57	137.786 ± 0.013	−85 ± 15	4.45 ± 1.07	$(4.01^{-1.94}_{+3.32}) \times 10^{-6}$	−7.6 ± 2.6	$2.71^{-0.59}_{+0.66}$
Allende	C30	4567.32 ± 0.42	137.786 ± 0.013	−58 ± 9¶	4.00 ± 2.73	$(3.92^{-2.95}_{+4.53}) \times 10^{-6}$	−12.1 ± 2.9	$2.73^{-0.71}_{+1.29}$
NWA 5697	C1	4566.67 ± 0.43	137.786 ± 0.013	−60 ± 9¶	8.16 ± 1.03	$(1.48^{-0.48}_{+0.67}) \times 10^{-5}$	−10.7 ± 1.6	$1.33^{-0.48}_{+0.48}$
NWA 5697	3-C5*	4566.20 ± 0.63	137.807 ± 0.026	−50 ± 15	8.85 ± 1.83	$(2.52^{-1.24}_{+2.23}) \times 10^{-5}$	−11.1 ± 2.9	$0.78^{-0.68}_{+0.70}$
NWA 5697	C3	4566.02 ± 0.26	137.786 ± 0.013	−87 ± 9¶	8.12 ± 2.76	$(2.74^{-1.09}_{+1.30}) \times 10^{-5}$	−7.3 ± 3.1	$0.69^{-0.44}_{+0.54}$
NWA 5697	11-C1*	4565.84 ± 0.72	137.779 ± 0.029	−10 ± 11	5.55 ± 1.84	$(2.22^{-1.35}_{+2.83}) \times 10^{-5}$	−12.5 ± 2.9	$0.91^{-0.80}_{+0.86}$

Notes:
TC, time of crystallization.
* Chondrules with measured $^{238}U/^{235}U$ from Bollard et al. (2017).
¶ $\mu^{54}Cr$ data from Connelly et al (2012).

$^{25}Mg^{\pm}$ for 10 s, $^{26}Mg^{\pm}$ for 10 s, and $^{27}Al^{\pm}$ for 1 s. The excess of radiogenic ^{26}Mg, denoted as $\mu^{26}Mg^*$, expressed in the μ notation (parts per million deviations from a standard) was calculated using an exponential fractionation law as follows:

$$\mu^{26}Mg* = \mu^{26}Mg_{sample} - \left[\left(1+\frac{\mu^{25}Mg_{sample}}{10^6}\right)^{\frac{1}{0.511}} - 1\right] \times 10^6 - \beta + \left[\left(1+\frac{\mu^{25}Mg_{std}}{10^6}\right)^{\frac{1}{0.511}} - 1\right] \times 10^6 - \left[\left(1+\frac{\mu^{25}Mg_{std}}{10^6}\right)^{\frac{1}{\alpha_{SIMS}}} - 1\right] \times 10^6,$$

where $\mu^{25,26}Mg_{sample} = [(^{25,26}Mg/^{24}Mg)_{sample}/(^{25,26}Mg/^{24}Mg)_{ref.} - 1] \times 10^6$ and $\mu^{25}Mg_{std} = [(^{25}Mg/^{24}Mg)_{std}/(^{25}Mg/^{24}Mg)_{ref.} - 1] \times 10^6$. The instrumental mass fractionation, α_{SIMS}, and an instrumental offset, β, were determined through measurements of terrestrial standards of Takashima augite, Russian spinel, chromite from the Wakamatsu mine (Cr# ~0.46), SanCarlos olivine, and Miyakejima anorthite. Detailed procedures of the corrections and error estimations are described elsewhere (Itoh et al., 2008; Kawasaki et al., 2017). The analytical errors (2SE) for $\mu^{26}Mg^*$ ranged from 70-140 ppm for olivine, 110–220 ppm for spinel, and 850–3000 ppm for plagioclase and mesostasis. The relative sensitivity factor (RSF) for aluminum and magnesium was determined through San Carlos olivine and Miyakejima anorthite measurements for olivine and Al-rich phases (plagioclase and mesostasis), respectively. The RSF for aluminum and magnesium of spinel in chondrules could not be determined, because spinels show variable RSFs depending on chemical compositions (0.84 (Cr-free) and 1.36 to 1.77 (Cr-bearing)). Therefore, instead of the SIMS measurements, we determined $^{27}Al/^{24}Mg$ ratios of spinel in chondrules by quantitative elemental analysis using an energy dispersive X-ray spectrometer (EDS, Oxford X-Max 150) installed on a field emission type scanning electron microscope (SEM, JEOL JSM-7000F) at Hokkaido University. These measurements have been made at the same positions on the SIMS spots using a rastered electron beam before the SIMS measurements. A 15 keV electron beam probe with current of 0.3 nA was employed. The sample was coated with a carbon thin film (~20 nm) for the EDS analyses. We conducted the EDS elemental analyses of interesting areas using the company installed software (Oxford AZtec) before the gold coating and subsequent SIMS isotope measurements. The analytical error of the elemental EDS analysis was assigned as statistical error calculated from total X-ray counts. Uncertainties of $^{27}Al/^{24}Mg$ ratios of spinel are estimated to be 0.02 to 0.05 in this study. For the oxygen isotope measurements, we used a $^{133}Cs^+$ primary beam (20 keV, 200 pA) with a diameter of ~5 μm. Negative secondary ions ($^{16}O^-$, $^{17}O^-$, and $^{18}O^-$) were measured by combination of multicollection mode and peak-jumping mode. $^{16}O^-$ was measured using a Faraday cup ($10^{11}\Omega$, designed for L1), while $^{17}O^-$ and $^{18}O^-$ were measured sequentially using a single axial electron multiplier. The mass resolution

of M/ΔM for $^{17}O^-$ and $^{18}O^-$ was set at ~6000 to ensure that the contribution of $^{16}OH^-$ to $^{17}O^-$ was negligible, while that for $^{16}O^-$ was ~2000. The secondary ion intensity of $^{16}O^-$ was $\sim 6.9 \times 10^7$ cps. The measurement sequence of one cycle is as follows: (1) $^{16}O^-$ and $^{17}O^-$ were measured for 2 s, but the $^{16}O^-$ intensity was not used for isotope ratio determination because of compensation of start-up-time-constant of the Faraday cup, (2) $^{16}O^-$ and $^{17}O^-$ were measured simultaneously for 2 s, and subsequently (3) $^{18}O^-$ was measured for 2 s. The measurements consisted of 16 cycles of these counting sequences. Russian spinel ($\delta^{18}O = 8.5$ ‰) and San Carlos olivine ($\delta^{18}O = 5.2$ ‰) were used as reference materials to correct the instrumental mass fractionation for oxide minerals and silicate minerals, respectively. Matrix effects for mass fractionations among silicate minerals would be smaller than 1 ‰/amu

Table 3
Oxygen isotopic compositions of mineral phases in the eight chondrules.

Chondrule	Phase	$\delta^{17}O$ (‰)	2σ	$\delta^{18}O$ (‰)	2σ	$\Delta^{17}O$ (‰)	2σ
C30	Cr-Sp	2.7	3.6	4.6	3.6	0.3	3.9
	Cr-Sp	1.9	2.7	4.1	2.7	−0.2	2.8
	Cr-Sp	1.5	2.9	3.3	2.5	−0.2	3.2
	Ol	1.3	1.9	3.9	2	−0.8	2.2
	Ol	0.8	1.2	2.3	1.2	−0.4	1.2
	Ol	3.4	1	3.4	1.1	1.6	1.1
	Ol	2.6	1.6	4.1	1.1	0.5	1.5
	Ol	4	1.3	3.8	1.3	2	1.4
	Px	1.9	2.1	4.5	1.7	−0.4	2.3
	Average	2.2	1.9	3.8	1.3	0.3	1.8
	Wtd Avg	2.5	1.0	3.6	0.5	0.6	0.6
2-C1	Ol	3.1	2.0	4.3	1.1	0.9	1.8
	Ol	2.4	1.4	3.2	1.4	0.8	1.6
	Ol	2.0	1.0	3.0	1.3	0.4	1.2
	Mes	2.0	1.1	2.4	1.2	0.8	1.0
	Mes	0.8	1.3	1.1	1.1	0.2	1.4
	Mes	0.2	1.4	1.4	1.1	−0.5	1.3
	Px	−0.6	1.3	0.8	1.0	−1.0	1.1
	Px	−0.3	1.1	0.5	1.0	−0.5	1.0
	Px	0.2	1.5	1.4	1.2	−0.5	1.5
	Average	1.1	2.5	2.0	2.4	0.0	1.4
	Wtd Avg	1.0	0.9	1.8	1.0	0.0	0.4
5-C2	Ol	1.8	1.6	4.9	1.3	−0.8	1.4
	Ol	4.4	1.3	5.3	1.3	1.6	1.5
	Ol	4.3	1.2	5.3	1.5	1.5	1.3
	Ol	1.8	1.6	4.9	1.3	−0.8	1.4
	Mes	4.4	1.6	4.3	1.3	2.2	1.5
	Mes	3.2	1.4	3.6	1.5	1.3	1.4
	Cr-Sp	4.0	1.6	4.4	1.0	1.7	1.4
	Cr-Sp	2.9	1.8	4.4	0.9	0.6	1.8
	Px	1.5	1.4	3.2	1.4	−0.1	1.5
	Px	2.2	1.9	3.4	1.1	0.4	1.8
	Px	2.5	1.7	5.0	1.1	−0.1	1.8
	Px	4.4	1.2	5.9	1.4	1.4	1.2
	Average	3.1	2.2	4.6	1.6	0.7	1.9
	Wtd Avg	3.3	0.8	4.5	0.4	0.8	0.7
5-C10	Ol	3.9	1.1	6.4	1.1	0.6	1.0
	Ol	4.0	1.6	6.6	1.1	0.5	1.6
	Ol	4.4	1.8	6.7	1.3	0.9	1.9
	Mes	4.9	1.6	7.5	1.4	1.0	1.9
	Mes	2.8	1.8	4.4	1.4	0.5	1.7
	Mes	4.4	1.8	7.3	1.3	0.7	1.8
	Cr-Sp	0.9	1.6	2.9	0.8	−0.6	1.7
	Px	2.6	1.8	5.7	1.3	−0.3	1.8
	Px	3.4	1.6	5.1	1.1	0.7	1.7
	Px	2.4	1.3	2.9	1.0	0.9	1.4
	Average	3.4	2.3	5.5	3.2	0.5	1.0
	Wtd Avg	3.4	0.8	5.1	1.3	0.5	0.5

(*continued on next page*)

Table 3 (*continued*)

Chondrule	Phase	$\delta^{17}O$ (‰)	2σ	$\delta^{18}O$ (‰)	2σ	$\Delta^{17}O$ (‰)	2σ
C1	Ol	3.2	2.3	6.5	1.2	−0.2	2.4
	Ol	6.1	2.5	8.0	1.2	2.0	2.6
	Ol	6.3	2.3	7.3	1.2	2.5	2.4
	Ol	4.1	2.2	7.2	1.2	0.4	2.3
	Px	5.7	2.7	5.5	1.4	2.8	2.8
	Px	6.5	2.5	6.4	1.2	3.2	2.6
	Px	4.3	2.6	6.0	1.1	1.2	2.7
	Px	3.3	2.4	7.3	1.3	−0.5	2.5
	Mes	14.3	2.3	16.5	1.3	5.8	2.4
	Mes	12.8	2.2	15.6	1.2	4.7	2.3
	Mes	11.2	3.0	15.6	1.4	3.1	3.0
	Mes	12.2	2.1	13.9	1.0	5.0	2.1
	Average	7.5	7.7	9.7	8.3	2.5	3.9
	Wtd Avg	7.7	2.6	9.7	2.7	2.6	1.4
3-C5	Ol	1.6	1.1	5.0	1.2	−1.0	1.3
	Ol	2.4	1.4	4.7	1.6	−0.1	1.5
	Ol	2.8	1.0	4.3	1.1	0.6	1.0
	Mes	2.0	1.3	3.5	1.2	0.2	1.3
	Mes	2.0	1.2	3.5	1.1	0.2	1.3
	Mes	3.1	1.4	3.9	1.6	1.0	1.9
	Cr-Sp	2.3	1.0	3.9	0.8	0.2	1.0
	Px	0.6	1.4	2.6	1.1	−0.7	1.4
	Px	1.7	1.4	2.8	1.4	0.3	1.4
	Px	0.6	1.3	3.1	1.0	−1.0	1.4
	Average	1.9	1.5	3.8	1.6	−0.1	1.3
	Wtd Avg	1.9	0.4	3.8	0.6	−0.1	0.4
C3	Ol	4.6	2.1	6.7	1.1	1.1	2.2
	Ol	5.8	2.3	7.5	1.0	1.9	2.3
	Ol	4.2	2.1	7.4	1.0	0.4	2.1
	Px	5.0	2.4	5.6	1.2	2.1	2.5
	Px	2.2	2.9	4.9	1.4	−0.4	3.0
	Mes	4.2	2.7	6.2	1.4	0.9	2.8
	Mes	3.3	2.5	4.8	1.3	0.8	2.6
	Mes	3.9	2.2	4.7	1.2	1.5	2.3
	Mes	5.2	2.9	5.2	1.5	2.5	3.0
	Average	4.3	2.1	5.9	2.1	1.2	1.7
	Wtd Avg	4.3	0.8	6.1	0.9	1.2	0.8
11-C1	Ol	2.0	1.8	5.1	1.0	−0.7	1.9
	Ol	3.9	1.2	3.2	1.4	2.2	1.4
	Ol	3.5	1.1	5.2	1.0	0.8	1.2
	Ol	3.0	1.3	5.7	1.1	0.1	1.3
	Mes	4.9	1.2	8.1	1.1	0.7	1.3
	Mes	4.4	1.0	5.1	1.0	1.7	1.0
	Cr-Sp	2.2	1.1	4.7	0.9	−0.3	1.1
	Cr-Sp	2.7	1.3	3.7	1.1	0.8	1.4
	Cr-Sp	2.5	1.1	5.2	0.8	−0.2	1.2
	Px	1.7	1.3	3.4	1.0	−0.1	1.2
	Px	2.1	1.2	3.1	1.2	0.5	1.3
	Average	3.0	2.0	4.8	2.8	0.5	1.7
	Wtd Avg	3.1	0.7	4.9	0.9	0.6	0.6

Notes: Ol, olivine, Cr-Sp, chrome spinel, Px, pyroxene, Mes, mesostasis, Wtd Avg, weighted average.

(Yurimoto et al., 2011), which are comparable to the analytical errors in this study. Analytical errors for $\delta^{17}O$, $\delta^{18}O$, and $\Delta^{17}O$ were typically 1.5‰, 1.2‰, and 1.5‰ (2σ), respectively. Following SIMS work, all analyzed materials were scrutinized using the SEM to ensure that no analysis was performed on cracked and/or overlapping minerals.

2.2. Bulk Mg and ^{54}Cr isotope measurements

Small aliquots of approximately 1–2 mg of each individual chondrules were digested with mixtures of concentrated HF-HNO_3 acids for 2 days using Parr bombs at 210 °C, after which they were re-dissolved in aqua regia overnight.

Magnesium and chromium were purified from sample matrices by ion exchange chromatography based on previously developed protocols (Bizzarro et al., 2011; Schiller et al., 2014; Larsen et al., 2016a; van Kooten et al., 2016) and adapted for the typically smaller sample sizes processed in this study. In summary, Mg was separated using a six-step purification scheme that combines cation, anion, TODGA and Ni-spec resins (Bizzarro et al., 2011). The Cr-rich separate was retrieved from the second step of the Mg chemical purification and further processed using a miniaturized cation exchange resin column (AG50X8 200-400 mesh, 100 μL resin volume). The sample was dissolved in a small volume of 1 M HNO_3 with 0.1% H_2O_2 and left for ≥5 days at room temperature in order to promote formation of Cr^{3+} species with a high affinity for the cation exchange resin (Larsen et al., 2016a). Following this pretreatment, the sample was diluted to 0.1 M HNO_3 and then loaded on the column. Sodium, potassium, and organics were eluted with 0.1 M HNO_3 followed by 1 M HF to remove potential remaining high field strength elements and Fe. The sample Cr was finally eluted in a small volume of 6 M HCl. We checked all washes to ensure that the Cr-yield was >95%, and if necessary reprocessed any fractions with significant Cr-fractions to ensure the yield target and thereby avoid artifacts due to loss of fractionated Cr. Afterwards, the Cr separates were dissolved in concentrated aqua regia for 1 week and concentrated HNO_3 for 3 days at 130 °C to remove any remaining organics. For comparison, chemistry yields for Mg were >99%. Total Mg and Cr procedural blanks were less than 5 ng and 0.5 ng, respectively, and, thus, negligible for all samples analyzed in this study.

The isotopic composition of the purified Mg was determined using the Neptune Plus Multi-Collector Inductively Coupled Plasma Mass Spectrometer (MC-ICPMS) at the Centre for Star and Planet Formation, Natural History Museum of Denmark, with the full analytical procedures reported in Bizzarro et al. (2011). Samples were aspirated into the plasma source by means of an Apex sample introduction system with an uptake rate of ~50 μL/min and the Mg isotope composition was measured in high-resolution mode ($M/\Delta M > 5000$). Using this approach, the sensitivity of the instrument was ~200 V ppm^{-1} and samples were typically analyzed with a signal intensity ranging from 35 to 100 V on mass ^{24}Mg. Single analyses comprised 1667 s of data acquisition followed by 570 s of baseline measurements obtained on-peak. Each sample was bracketed by standard analyses and systematically analyzed ten times, with the intensity of the sample and standard matched to 5%. The $^{26}Mg^*$ data are reported in the μ-notation as relative deviations from the DTS-2b standard ($\mu^{26}Mg^*$ DSM-3 = 0.9 ± 1.7 ppm, 2SD, Bizzarro et al., 2011) according to the following formula:

$$\mu^{26}Mg^* = [(^{26}Mg/^{24}Mg)_{sample}/(^{26}Mg/^{24}Mg)_{standard} - 1] \times 10^6$$

where the $^{26}Mg/^{24}Mg$ values reflect the internally normalized ratios where $^{25}Mg/^{24}Mg = 0.126896$ (Bizzarro et al., 2011) and using the exponential mass fractionation law (Young and Galy, 2004). All Mg data reduction was conducted off-line using the Iolite data reduction package (Paton et al., 2011) that runs within Igor Pro and changes in mass bias with time were interpolated using a smoothed cubic spline. For each analysis, the mean and standard error of the measured ratios were calculated using a 3 SD threshold filter to reject outliers. Individual analyses (10) of a sample were combined to produce an average weighted by the propagated uncertainties of individual analyses and reported final uncertainties are the 2SE of the mean. The external reproducibility of our measurements using this method is 2.5 ppm for the $\mu^{26}Mg^*$ value (Bizzarro et al., 2011). The $^{27}Al/^{24}Mg$ ratios were measured on an X-series ICP-MS at the Centre for Star and Planet Formation and are accurate to 2%.

The isotopic composition of the purified Cr was determined with the Triton Thermal Ionization Mass Spectrometer (TIMS) at the Centre for Star and Planet Formation, Natural History Museum of Denmark, using a sample-standard bracketing approach. Cr was dissolved and heat-pretreated for >1 h in ~10 M HCl prior to mixing into a silica gel-boric acid-aluminum slurry that was subsequently loaded onto single W-filaments (pre-outgassed for 2 hours at 4.5 A). Prior to loading, the filaments were heated with a ~2 A current and dabbed with the edge of a piece of parafilm to prevent the sample slurry from spreading too far laterally on the filament. Samples were then loaded at a current of ~1.5–2 A to provide rapid dry-down without actual boiling. During analysis, the filaments were automatically heated, focused and trimmed to ~250 mV ^{52}Cr before rapid ramping to ~10 V ^{52}Cr using the total evaporation mode control. This voltage was maintained until the mass spectrometer software could no longer support it with a current ramp of ~8 mA/sec. During analysis, ^{50}Cr, ^{52}Cr, ^{53}Cr, ^{54}Cr, ^{51}V and ^{56}Fe were collected on Faraday cups linked to 10^{11} Ohm resistors, while ^{49}Ti was collected on a Faraday cup linked to a 10^{12} Ohm resistor. Data reduction was carried out off-line utilizing the Iolite data reduction package, and included correction for ^{50}Ti, ^{50}V and ^{54}Fe. We only included the emission where ^{52}Cr was stable at ~10 V. We never observed any significant ^{49}Ti or ^{51}V, while ^{56}Fe was typically <10 μV. Each sample measurement consists of the average and standard error of at least 10 individual ~15 ng filament loads, calculated using a 3 SD outlier rejection scheme. Sample analyses were interspaced with analyses of ~15 ng filament loads of the SRM-3112a standard, measured under the same conditions as the samples. Individual analyses typically consist of 500 s to 1500 s of data acquisitions, with typical internal precision of 20 ppm for the $^{54}Cr/^{52}Cr$ ratio. Electronic baselines were measured during the 4 minute heating. The $^{54}Cr/^{52}Cr$ data are reported in the μ notation according to the following formula:

$$\mu^{54}Cr = [(^{54}Cr/^{52}Cr)_{sample}/(^{54}Cr/^{52}Cr)_{standard} - 1] \times 10^6$$

where the $^{54}Cr/^{52}Cr$ values reflect the internally normalized values using the exponential mass fractionation law with $^{52}Cr/^{50}Cr = 19.2832$ (Trinquier et al., 2008). This approach provides several advantages as compared to traditional methods (i.e. Trinquier et al., 2008). First and foremost, total evaporation mode ensures rapid and reproducible measurement of >90% of the transmitted sample, which is

critically important for measurements of small samples such as clasts and small chondrules. The total evaporation mode also stabilizes the sample current within a very narrow intensity window, which alleviates the need for frequent baseline measurements; variations in baselines and other machine parameters are instead corrected by the standard bracketing approach. Finally, the dilution across multiple filaments allows repeat measurements and minimizes the impact of filament poisoning by remaining resin-derived organics.

The accuracy and external reproducibility of our measurements was determined by repeated analyses of column-processed Ivuna CI chondrite and terrestrial rock standards (DTS-2b and BHVO-2), using quantities of magnesium and chromium comparable to that present in the smallest samples analyzed in our study. The Mg and Cr isotope data reported in this study were collected at the same time and using the same protocols as outlined in van Kooten et al. (2016) and, as such, we refer the reader to Table S4 of van Kooten et al. (2016) where the results of the column-processed Ivuna CI chondrite and terrestrial rock standards are reported. In summary, the five sample digestions of the Ivuna CI chondrite yield an average μ^{26}Mg* of 4.7 ppm, which is identical to that reported by Larsen et al. (2011). Moreover, the external reproducibility of the five aliquots of Ivuna analysed here corresponds to 2.9 ppm, which is similar to that of 2.5 ppm inferred for our method (Bizzarro et al., 2011). The analyses of two aliquots of the DTS-2b rock standard yield a terrestrial μ^{26}Mg* composition. Five column-processed aliquots of the DTS-2b yielded μ^{54}Cr consistent with the terrestrial composition, with an external reproducibility of 12 ppm. Finally, one analysis of the Ivuna CI chondrite yields a μ^{54}Cr value of 159 ± 14 ppm, which is identical to literature data (Trinquier et al., 2007). Thus, we conclude that the Mg and Cr isotope measurements presented in our study are accurate within their stated uncertainties.

2.3. Thermal models

Thermal modeling using ^{26}Al heat production of an ordinary chondrite type of source rock (density = 3800 kg m^{-3} (Lodders and Fegley 1998), Al = 1.13 wt% (Hutchison 2004)) was performed using an analytical solution to the heat equation for a sphere (Hevey and Sanders 2006; Larsen et al., 2016b). The model assumes instantaneous accretion at 1 AU, in the context of the viscous accretion disk thermal evolution model of Boss and Ciesla (2014) with a progressive decrease in disk temperature, starting with an initial ambient temperature of 1500 K and evolving to temperatures of 250 K after 1 Myr. We consider a large ordinary chondrite type planetesimal (100 km in radius) with onset of silicate melting at 1350 K (McCoy et al., 2006) and assume efficient metal-silicate differentiation at >50% melting, corresponding to a peak temperature of 1650 K (Mare et al., 2014). We use an ^{26}Al decay energy of 3.12 MeV per atom (Castillo-Rogez et al., 2009). The model does not consider the thermal consequences of melt migration nor incremental accretion. Melt migration would result in lower peak temperatures and, thus, higher inferred $(^{26}Al/^{27}Al)_0$ to achieve melting, while incremental accretion does not significantly change the resulting thermal profile within the accreting planetesimal (Larsen et al., 2016b), but depends on the evolution of the ^{26}Al abundance in the disk.

3. RESULTS

The oxygen isotope compositions of the mineral phases from individual chondrules used for Al-Mg systematics are presented in Table 3. The various mineral phases have identical Δ^{17}O values within uncertainty indicating that the minerals from individual chondrules were not related to refractory inclusions (CAIs and AOAs) and were formed during chondrule formation. Thus, the ^{26}Al-^{26}Mg systems should define internal isochron relationships for formation of individual chondrules.

Given the possibility that Al-rich phases of Allende chondrules experienced late-stage disturbance of their ^{26}Al-^{26}Mg systematics during thermal metamorphism on the CV parent body (Hutcheon et al., 2009; Kawasaki et al., 2015), we restricted our analysis of the C30 chondrule to minerals believed to be more resistant to thermal resetting such as olivine and Cr-spinel. Spinel is considered to be a primary phase in chondrules (Kimura et al., 2006) consistent with the lack of Fe-Mg zoning in coexisting olivine crystals. Multiple analyses of Cr-spinels, olivine grains and a single bulk rock fraction define a statistically significant isochron corresponding to an initial ^{26}Al/^{27}Al ratio of $(4.00 \pm 2.73) \times 10^{-6}$ at the time of crystallization of this chondrule (Fig. 1). This initial is much lower than the predicted $[^{26}Al/^{27}Al]_0$ of $(5.25 \pm 1.73) \times 10^{-5}$ inferred from its absolute U-corrected Pb-Pb age of 4567.32 ± 0.42 Ma, assuming ^{26}Al homogeneity in the solar protoplanetary disk with the canonical $[^{26}Al/^{27}Al]_0$ ratio. This corresponds to an age mismatch between the ^{26}Al-^{26}Mg and Pb-Pb ages of $2.73^{+1.39}_{-0.71}$ Myr. For NWA5697, the majority of initial ^{26}Al/^{27}Al values are inferred from isochron relationships based on bulk rock fractions, olivine, spinel and Al-rich mesostasis. Inclusion of the mesostasis is justified as the ^{26}Al-^{26}Mg systematics of pristine unequilibrated ordinary chondrites of low petrologic type chondrites such as NWA5697 (L3.10, Bollard et al., 2017) are typically unaffected by secondary disturbance. The seven chondrules define resolvable initial ^{26}Al/^{27}Al ratios at the time of their crystallization ranging from $(4.45 \pm 1.07) \times 10^{-6}$ to $(8.85 \pm 1.83) \times 10^{-6}$, which is similar to that recorded by the majority of chondrules from unequlibrated ordinary chondrites (Huss et al., 2001; Mostefaoui et al., 2002; Rudraswami and Goswami, 2007; Villeneuve et al., 2009; Pape et al., 2019). The initial ^{26}Al/^{27}Al ratios at the time of crystallization of the chondrules are much lower than that predicted by their Pb-Pb ages assuming ^{26}Al homogeneity, corresponding to a mismatch between the ^{26}Al-^{26}Mg and U-corrected Pb-Pb ages ranging from $0.69^{+0.54}_{-0.44}$to $2.71^{+0.66}_{-0.63}$ Myr. The $[^{26}Al/^{27}Al]_0$ in the chondrule precursors at the time of CAI formation span from $2.74^{+1.30}_{-1.09} \times 10^{-5}$ to$4.01^{+3.32}_{-1.94} \times 10^{-6}$. The ^{26}Al-^{26}Mg data are reported in Table 4 whereas the ages and inferred

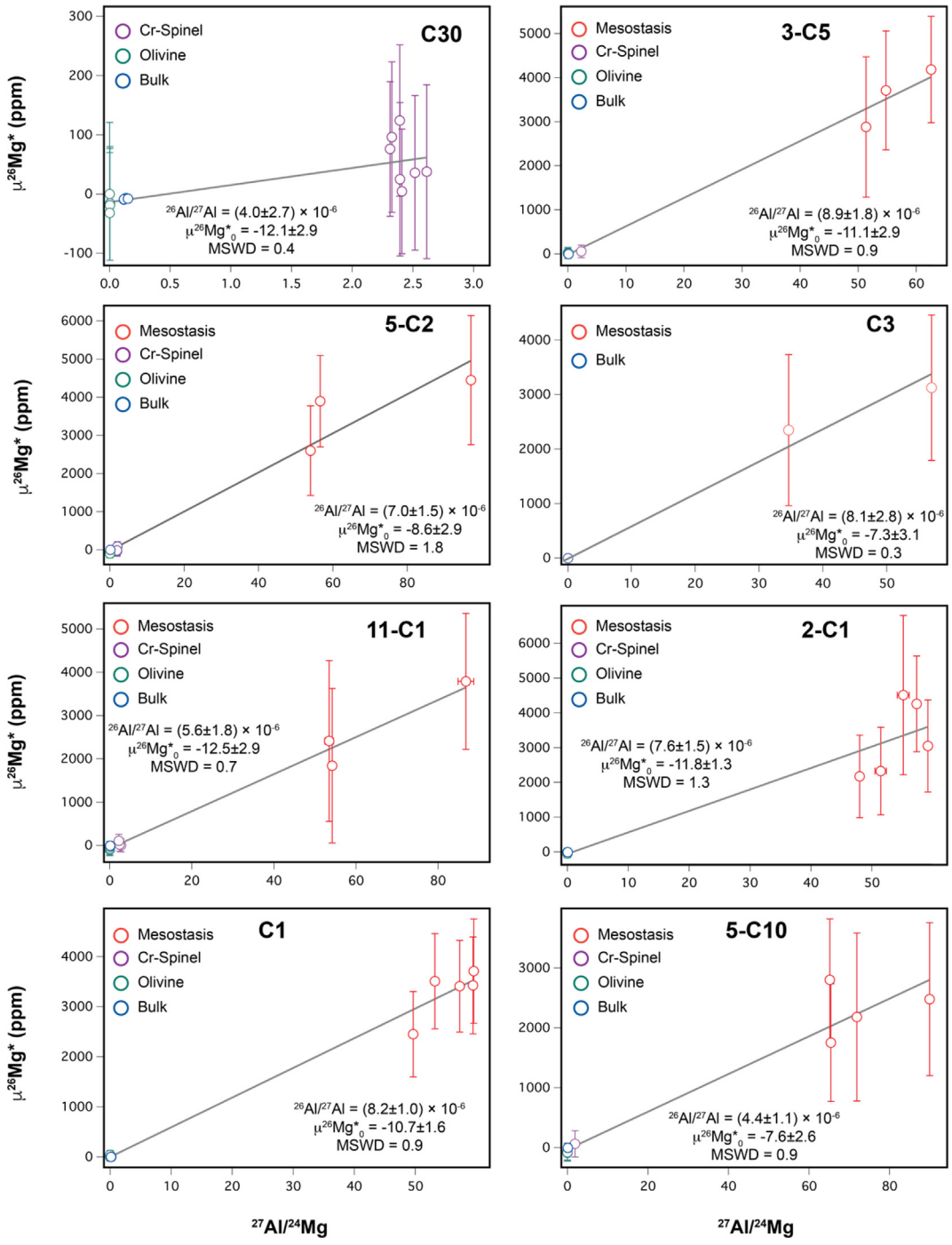

Fig. 1. ^{26}Al-^{26}Mg variations diagrams and regression summaries of chondrules investigated in this study.

$^{26}Al/^{27}Al$ values of individual chondrules analysed here are summarized in Table 2.

The eight chondrules investigated here, namely seven from the NWA 5697 ordinary chondrite and one from the Allende carbonaceous chondrites, record $\mu^{54}Cr$ values ranging from 7 ± 15 ppm to -85 ± 15 ppm. These compositions are consistent with an inner Solar System origin for these objects and, as such, we interpret that these chondrules formed in the terrestrial planet formation region (Trinquier et al., 2007; Trinquier et al., 2009; Warren, 2011). Although chondrule C30 is from the Allende CV chondrite, which is inferred to have accreted beyond the orbit of Jupiter (Warren, 2011; Olsen et al., 2016), the $\mu^{54}Cr$ composition of this chondrule is not consistent with an outer Solar System origin. The existence of a ^{54}Cr-poor chondrule population amongst Allende chondrules has been demonstrated by Olsen et al. (2016), which is interpreted as reflecting outward mass transport of inner Solar

Table 4
Mineral and bulk ^{26}Al-^{26}Mg systematics of the eight chondrules investigated.

Chondrule	Phase	^{27}Al/^{24}Mg	2σ	μ^{26}Mg* (ppm)	2σ
C30	Mes	95.892	2.866	−198.0	2584.2
	Mes	93.399	2.781	975.5	3013.8
	Cr-Sp	2.614	0.033	37.6	146.8
	Cr-Sp	2.517	0.028	35.8	130.4
	Cr-Sp	2.410	0.028	4.5	105.3
	Cr-Sp	2.394	0.027	24.8	129.5
	Cr-Sp	2.392	0.028	124.1	127.8
	Cr-Sp	2.327	0.027	96.2	127.1
	Cr-Sp	2.312	0.026	76.1	113.6
	Ol	0.005	0.001	−16.0	96.0
	Ol	0.004	0.001	−19.0	96.0
	Ol	0.002	0.001	−32.0	102.0
	Ol	0.002	0.001	0.0	121.0
	Bulk 1	0.119	0.001	−9.5	2.5
	Bulk 2	0.137	0.013	−6.9	2.5
	Bulk 3	0.120	0.013	−8.9	2.5
	Bulk 4	0.153	0.013	−8.0	2.5
	Bulk avg	0.132	0.013	−8.3	2.3
2-C1	Mes	59.194	0.546	3046.8	1323.6
	Mes	57.359	0.132	4258.6	1378.6
	Mes	55.160	0.962	4511.6	2289.9
	Mes	51.448	0.929	2325.5	1261.7
	Mes	47.989	0.117	2170.7	1187.7
	Ol	0.002	0.001	−50.8	119.5
	Ol	0.002	0.001	−10.9	120.2
	Bulk Ol	0.003	0.013	−9.7	2.5
	Bulk	0.062	0.013	−9.0	2.5
5-C2	Mes	97.161	0.786	4448.6	1691.6
	Mes	56.615	0.493	3897.2	1198.0
	Mes	53.986	0.422	2597.8	1173.7
	Cr-Sp	2.024	0.021	83.9	129.0
	Cr-Sp	1.926	0.020	−34.5	138.3
	Cr-Sp	1.907	0.022	−16.7	134.4
	Ol	0.003	0.001	−79.9	111.6
	Ol	0.003	0.001	−69.2	108.0
	Ol	0.001	0.001	−102.1	111.4
	Bulk	0.124	0.013	−2.1	2.5
5-C10	Mes	89.916	0.435	2477.8	1276.4
	Mes	71.877	0.339	2179.7	1403.3
	Mes	65.411	0.326	1751.4	981.5
	Mes	65.155	0.339	2800.0	1015.9
	Cr-Sp	1.892	0.054	64.2	218.5
	Ol	0.005	0.001	−64.0	140.4
	Ol	0.004	0.001	−79.9	137.9
	Ol	0.000	0.001	−87.1	139.8
	Ol	0.000	0.001	−79.0	134.9
	Bulk	0.099	0.013	−4.4	2.5
C1	Mes	59.564	0.055	3708.8	1041.7
	Mes	59.447	0.155	3424.9	969.3
	Mes	57.270	0.054	3408.0	915.7
	Mes	53.203	0.167	3509.2	951.7
	Mes	49.653	0.088	2449.2	854.2
	Ol	0.006	0.004	19.0	80.0
	Ol	0.003	0.003	−2.0	87.0
	Ol	0.002	0.002	16.0	74.0
	Ol	0.002	0.001	40.0	87.0
	Bulk 1	0.173	0.003	1.6	2.5
	Bulk 2	0.163	0.003	−1.0	2.5
	Bulk 3	0.145	0.003	−3.6	2.5

(*continued on next page*)

Table 4 (*continued*)

Chondrule	Phase	$^{27}Al/^{24}Mg$	2σ	$\mu^{26}Mg^*$ (ppm)	2σ
	Bulk 4	0.199	0.003	−0.8	2.5
	Bulk 5	0.141	0.004	−1.9	2.5
	Bulk avg	0.164	0.047	−1.1	3.8
3-C5	Mes	62.567	0.121	4181.6	1207.8
	Mes	54.791	0.158	3708.4	1348.0
	Mes	51.355	0.077	2880.9	1593.0
	Cr-Sp	2.299	0.022	56.6	142.2
	Ol	0.002	0.001	16.4	118.4
	Ol	0.001	0.001	21.8	122.7
	Ol	0.001	0.001	9.0	118.4
	Bulk	0.105	0.013	−4.5	2.5
C3	Mes	57.018	0.313	3125.2	1334.0
	Mes	34.638	0.077	2348.4	1384.0
	Bulk	0.097	0.002	−1.7	2.5
11-C1	Mes	86.764	1.910	3789.0	1570.1
	Mes	54.187	0.313	1840.7	1782.8
	Mes	53.448	1.071	2414.1	1857.2
	Cr-Sp	2.745	0.024	3.6	149.5
	Cr-Sp	2.409	0.024	19.6	152.0
	Cr-Sp	2.221	0.051	105.0	153.2
	Ol	0.004	0.001	−92.3	136.1
	Ol	0.001	0.001	−49.2	97.5
	Ol	0.001	0.001	−41.2	91.9
	Ol	0.001	0.001	−99.3	137.5
	Ol	0.001	0.001	−37.4	91.6
	Ol	0.001	0.001	−62.7	94.6
	Ol	0.000	0.001	−84.7	136.2
	Ol	0.000	0.001	−41.7	135.4
	Bulk	0.104	0.013	−8.1	2.5

Notes: Ol, olivine, Cr-Sp, chrome spinel, Mes, mesostasis, Bulk Avg, bulk average.

System solids to the accretion region of carbonaceous chondrites, perhaps associated with the transport of CAIs. The absolute age of C30, indistinguishable from CAIs, is consistent with this interpretation. Thus, we conclude that the $\mu^{54}Cr$ systematics support an inner Solar System origin for all chondrules reported here.

4. DISCUSSION

4.1. A low initial $^{26}Al/^{27}Al$ ratio in chondrule precursors

Our new in situ ^{26}Al-^{26}Mg data clearly establish that the internal ^{26}Al-^{26}Mg systematics of our subset of inner Solar System chondrules from the Allende and NWA 5697 chondrites record relative ^{26}Al-^{26}Mg ages that are younger by ~0.7 to ~1.7 Myr compared to age differences based on their absolute ages defined by the U-corrected Pb-Pb dating method. We consider four scenarios to account for this mismatch: (i) the Pb-Pb age offsets are based on uranium-corrected Pb-Pb ages that are not accurate to their stated uncertainties (where the incorporation of uncertainties on U decay constants is not necessary when considering age offsets), (ii) the Pb-Pb dates and Al-Mg ages reflect different events and/or processes, (iii) $^{238}U/^{235}U$ variability in chondrule precursors and, lastly, (iv) the chondrules formed from precursor material with a lower initial abundance of ^{26}Al compared to the canonical value.

In the first scenario, we explore the possibility that the age variability or, alternatively, the preponderance of old ages inferred from Pb-Pb dating that results in the age mismatch is an artifact of the progressive step-leaching dissolution technique (Connelly and Bizzarro, 2009) used by Connelly et al. (2012) and Bollard et al. (2017), relative to more traditional approaches based on the analyses of separated mineral phases. However, three lines of evidence suggest that this is not the case. First, two independent estimates of the Pb-Pb age for the SAH99555 angrite using the step-leaching dissolution technique (Connelly et al., 2008) and a more traditional mineral separation approach (Amelin, 2008) yield ages that are concordant within 280,000 ± 405,000 years. Similarly, independent estimates for the timing of condensation of CAIs using different techniques (Amelin et al., 2010; Connelly et al., 2012) define ages that are within 140,000 ± 505,000 years. In both cases, the potential offset between the two techniques is well within the typical uncertainties of the chondrule ages reported here. Lastly, using the step-leaching technique, Bollard et al. (2015) report Pb-Pb ages for four individual chondrules from the Gujba metal-rich chondrite that are identical within 340,000 years. This chondrite is thought to have formed from a vapor-melt plume produced by a giant impact between planetary embryos, resulting in coeval ages of its various components (Krot et al., 2005).

It has recently been speculated that chondrule ages defined by the Pb-Pb system (i.e. Connelly et al., 2012; Bollard et al., 2017) may be inaccurate due to ^{222}Rn (half-life of 3.8 days) loss in the ^{238}U-^{206}Pb decay chain (Pape et al., 2019). Although no detailed modeling or specific mechanisms are provided by Pape et al. (2019), we identify three processes that, in theory, may have affected the inventory of ^{222}Rn in chondrules, namely: (1) instantaneous diffusional loss of ^{222}Rn caused by a flash heating event prior to parent-body accretion, (2) long-term diffusional loss of ^{222}Rn potentially both pre- and post-accretion, and (3) long-term loss of ^{222}Rn from chondrules related to recoil during the alpha decay of the parent nuclide ^{226}Ra.

The first process considers ^{222}Rn loss during transient heating events in the nebula in events where temperatures are elevated but do not reach the chondrule melting point. At radiogenic isotopic equilibrium of the ^{238}U decay series, the relative abundance of ^{222}Rn to ^{238}U is 2.3×10^{-12}. Given that the thermal processing of disk solids associated with the chondrule forming mechanism is thought to occur over timescales of hours to days (Scott, 2007), the loss of the small amounts of ^{222}Rn present in these brief events will be insignificant with respect to the total final inventory of radiogenic ^{206}Pb. As such, this mechanism cannot produce measurable offsets of ^{207}Pb/^{206}Pb ages.

With respect to the potential longer term radon diffusion, we note that there is no systematic correlation between the Pb-Pb ages of chondrules and the metamorphic grade of the host chondrites, precluding measurable ^{222}Rn loss associated with parent body processes. For example, Allende (CV3.6), NWA 5697 (L3.10) as well as various CR chondrites show a comparable range of chondrule ages despite their contrasting thermal histories (Connelly et al., 2012; Bollard et al., 2017). To assess low temperature ^{222}Rn loss from meteorites, Girault et al. (2017) recently reported significant emanations of ^{222}Rn in different meteoritic materials, which they attributed to present-day diffusion of ^{222}Rn produced in the decay series of ^{238}U. That ^{222}Rn is diffusing out of meteorites at room temperature today raises the concern that this may have been occurring over geological timescales to cause a measurable deficit in the final amount of radiogenic ^{206}Pb. Ignoring that Girault et al. (2017) stated that "*The radon-222 released inside the mineral grains or chondrules remains essentially trapped and undetectable*", their average reported bulk loss of $40 \pm 4\%$ of the total ^{222}Rn production in meteorites would result in highly anomalous ^{207}Pb/^{206}Pb ratios. If this occurred over the lifetime of the chondrule, a 40% loss of ^{206}Pb would correspond to ages of ~5300 Ma. However, Pb isotope measurements of chondrules, CAIs and matrix from a wide range of meteorites do not yield diagnostic highly-anomalous ^{207}Pb/^{206}Pb ratios and, therefore, offer no evidence for measurable ^{222}Rn loss. The fact that the measurements of Girault et al. (2017) of ^{222}Rn emanating from virtually U-free iron meteorites is comparable to that from chondrites is puzzling. In any case, it appears that current measurements of present-day ^{222}Rn emanation from meteorites cannot be used at face value to infer ^{222}Rn loss over the long term as suggested by Pape et al. (2019).

The recoil in opposing directions of the daughter ^{222}Rn isotope and complementary alpha particle resulting from the decay of ^{226}Ra has been considered as a mechanism for ^{222}Rn loss from solids. This requires that the daughter ^{222}Rn ends up in adjacent pore space or in a fission track that is interconnected to the pore space. In materials such as zircon with orders of magnitude higher U contents than chondrules, the fission track density may be high enough to allow for an interconnecting network to facilitate ^{222}Rn to the edge of the grain. Indeed, a range of 1.7–2.3% of the existing ^{222}Rn in three samples of zircon has been determined to be escaping from various grains sizes (Garver and Baskaran, 2004). With recoil distances for ^{222}Rn being ~35 nm (Ishimori et al., 2013), we can predict the amount of ^{222}Rn lost from a round, crack-free chondrule assuming a homogeneous distribution of U. A recoil distance of 35 nm requires that the parent ^{226}Ra must be within this distance from the edge of the chondrule for ^{222}Rn produced in this volume to exit the chondrule. A conservative approximation that half of the ^{222}Rn produced in this rim will exit the chondrule predicts that only 0.0009% of all ^{222}Rn produced in a 5 mm diameter chondrule will be lost. Losing this amount of ^{222}Rn from a chondrule is within our stated age uncertainties of 0.005% and would certainly not shift the age by ca. 1.7 Ma (0.037%). Furthermore, our routine procedure of removing the surrounding matrix from chondrules by a Dremel^{TM} tool is expected to remove at least 50 nm of the outer layer of the chondrule, thereby eliminating any concern of ^{222}Rn loss from the chondrule by this mechanism.

In addition to these theoretical arguments against ^{222}Rn loss in chondrules, we note the following points also support this conclusion. If ^{222}Rn loss from the outer rim of chondrules is a significant process in chondrules, a number of predictions can be made on its impact on their U-Pb systematics. First, the ^{222}Rn loss should be more prominent in small chondrules, given the higher surface to volume ratios. The Pb-Pb dated chondrules reported in Bollard et al. (2017) have diameters that range from 2.3 to 8 mm, representing a factor of 3.5 in size variability. Fig. 2 shows that no systematic relationship exists between the age and size of the chondrules. However, some of the chondrules investigated show the presence of cracks, which may enhance ^{222}Rn loss, depending on when the fragmentation occurred. A second prediction of ^{222}Rn loss is the lack of linearity in Pb-Pb isotope space given that the redistribution of ^{222}Rn will result in domains with varying radiogenic ^{207}Pb/^{206}Pb ratios. With ^{222}Rn loss concentrated in the outer surface of the chondrules, a large range in radiogenic ^{207}Pb/^{206}Pb ratios will be generated and easily detected using the step-leaching approach employed in Connelly et al. (2012) and Bollard et al. (2017). As a result, ^{222}Rn loss will result in a nonlinear array in Pb-Pb space with anomalously high ^{207}Pb/^{206}Pb ratios rather than shifted linear arrays corresponding to erroneously old ages as speculated by Pape et al. (2019). A third prediction of continuous ^{222}Rn loss from chondrules after accretion of the parent body is a lower radiogenic ^{207}Pb/^{206}Pb ratio in the matrix material surrounding the chondrules. However, the matrix of the

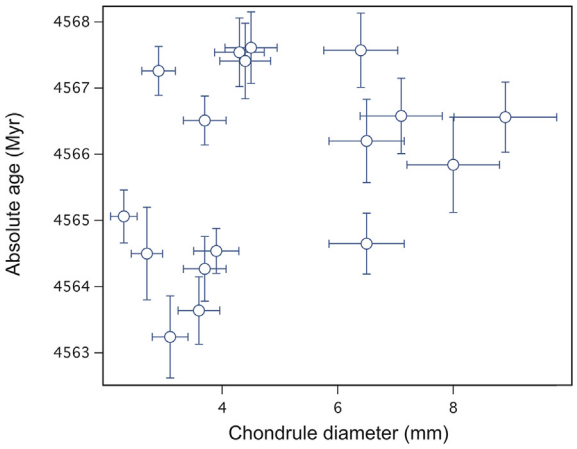

Fig. 2. Variation diagram depicting the chondrule ages and size. The chondrule size is defined by the diameter of the chondrules in millimeter, estimated from the elemental maps. A 10% uncertainty is assigned to the chondrule diameter. All data in this diagram are from Bollard et al. (2017).

pristine NWA 5697 chondrite, from which a significant number of the chondrules reported in Bollard et al. (2017) were extracted, shows no sign of anomalous uranogenic Pb (Connelly and Bizzarro, 2016). A fourth prediction of inhomogeneous ^{222}Rn loss is a randomization of the chondrules ages, including ages that are significantly older than the Solar System. However, none of the Pb-Pb ages reported so far are older than CAIs within uncertainty. Stated conversely, the observation that the oldest dated chondrules define ages identical to CAIs requires a precise amount of ^{222}Rn to be lost over a restricted time period for which no mechanism has been identified. A fifth prediction would be the randomization of chondrule ages. However, the ages of four chondrules from the CB meteorite Gujba return overlapping ages as predicted by their inferred formation by a single planetesimal impact event. Finally, Pape et al. (2019) also speculated that ^{222}Rn loss is enhanced in the chondrule mesostasis that is damaged by the radioactive decay of ^{26}Al. If correct, this predicts a correlation between the chondrules Pb-Pb ages and the total amount of ^{26}Al in the mesostasis. As the mesostasis of the chondrules investigated have Al contents within 5% (Bollard et al., 2017), this predicts that there should be a positive correlation between the Pb-Pb ages and measured ^{26}Al/^{27}Al ratios of individual chondrules. In contrast, the old chondrule population with Pb-Pb ages identical to CAIs records an average ^{26}Al/^{27}Al ratio at their time of crystallization ($[^{26}Al/^{27}Al]_{TC}$) of $(5.9 \pm 0.8) \times 10^{-6}$, which is lower than the ~1 Myr younger chondrule population recording an $[^{26}Al/^{27}Al]_{TC}$ ratio of $(7.7 \pm 0.6) \times 10^{-6}$. In summary, we submit that ^{222}Rn loss is not a viable mechanism to produce spuriously old Pb-Pb ages and that the chondrule Pb-Pb dates reported in Connelly et al. (2012) and Bollard et al. (2017) are not affected by ^{222}Rn loss.

In the second scenario, we explore the idea that the Pb-Pb and Al-Mg ages are dating distinct events or processes. For example, the uranium-corrected Pb-Pb dates reflect the timing of U/Pb fractionation of the precursor material whereas the younger ^{26}Al-^{26}Mg ages represent the last chondrule melting events. However, the petrology of the eight chondrules investigated here indicates that these objects represent crystallization products of completely or near-completely molten silicate liquids (Connelly et al., 2012; Bollard et al., 2017). Thus, the newly-formed crystallizing minerals (i.e. olivine, pyroxene, spinel, and mesostasis) will have acquired a homogenized isotopic composition, which is confirmed by the oxygen isotope homogeneity of the various phases within individual chondrules. Moreover, Bollard et al. (2017) recently demonstrated using secondary ionization mass spectrometry (SIMS) that the major reservoir of U and, hence, radiogenic Pb in chondrules is the mesostasis composed of plagioclase and high-Ca pyroxene. As such, the isochron relationship in ^{207}Pb/^{206}Pb–^{204}Pb/^{206}Pb space essentially represents a binary mixture of the radiogenic Pb residing in the mesostasis and a primitive, non-radiogenic Pb component or modern terrestrial Pb in the few chondrules lacking initial Pb. Given that the mesostasis is the Al-rich phase that essentially controls the slope of the isochron in the Al-Mg evolution diagrams, it is evident that the Pb-Pb and Al-Mg ages must reflect the timing of crystallization of the mesostasis and, hence, the last chondrule melting events.

An additional potential mechanism related to the second scenario is that the younger Al-Mg ages reflect selective disturbance of the Al-Mg system. However, the NWA 5697 chondrite is amongst the most pristine ordinary chondrites classified to date with a thermal metamorphism degree less than that of the LL 3.15 Bishunpur, which corresponds to a peak metamorphic temperature less than 300 °C (Rambaldi and Wasson, 1981). Indeed, analysis of the organic matter by Raman spectroscopy indicates that NWA 5697 is of petrologic type 3.10, that is, among the most pristine ordinary chondrites (Bollard et al., 2017). Thus, it is unlikely that the Al-Mg system records a secondary event given the negligible effect of self-diffusion of Mg at these temperatures (La Tourette and Wasserburg, 1998). Moreover, we note that the initial ^{26}Al/^{27}Al ratios inferred from NWA 5697 chondrules are comparable to those observed in the most pristine type 3 chondrites such as, for example, Semarkona, Bishunpur and Krymka (Huss et al., 2001; Mostefaoui et al., 2002; Rudraswami and Goswami, 2007; Villeneuve et al., 2009). Thus, we conclude that the Al-Mg ages faithfully reflect a pristine signal recording the last chondrule melting event.

The discovery of variability in the ^{238}U/^{235}U composition of CAIs up to ~34 ε-unit (Brennecka et al. 2010), corresponding to a ^{207}Pb-^{206}Pb age variation of ~5 Myr, opened the possibility that similar variations may exist in chondrules, which in principle could account for the age mismatch between the U-Pb and Al-Mg systems. However, Connelly et al. (2012) reported high-precision ^{238}U/^{235}U data that showed no variability between pristine chondrite and achondrite meteorites as well as three individual Allende chondrules, which led them to propose a solar ^{238}U/^{235}U value of 137.786 ± 0.013 (see Connelly et al., 2017; Connelly and Bizzarro, 2018 for in-depth discussion). More recently, Bollard et al. (2017) showed that the ^{238}U/^{235}U compositions of seven individual chondrules

from the NWA 5697 chondrite are also identical to the solar $^{238}U/^{235}U$ value within uncertainty of the measurements, confirming the lack of U-isotope variability in chondrules. In particular, four out of the eight chondrules for which we report Al-Mg data have measured U-isotope compositions that have been used to calculate their Pb-Pb ages, with the uncertainty associated with the $^{238}U/^{235}U$ measurements propagated in the quoted Pb-Pb dates. Thus, the age mismatch between that the Al-Mg and Pb-Pb ages cannot be related to U-isotope heterogeneity in chondrule precursors.

Our interpretation that final closure of the U-Pb and ^{26}Al-^{26}Mg systems must represent the last chondrule melting event can be further evaluated by comparing the observed present-day bulk Mg isotope compositions and intercepts of the ^{26}Al-^{26}Mg regressions defined by individual chondrules with that predicted by their Pb-Pb and ^{26}Al-^{26}Mg ages. Fig. 3 depicts the $\mu^{26}Mg^*$ evolution of the subset of chondrules analyzed here with respect to two contrasting models for the interpretation of the significance of the mismatch between the Pb-Pb and ^{26}Al-^{26}Mg ages. In the first model (yellow), we assume ^{26}Al homogeneity with a canonical $[^{26}Al/^{27}Al]_0$ ratio of at the time CAI formation of $(5.252 \pm 0.019) \times 10^{-5}$ (Larsen et al., 2011) and that the Pb-Pb dates represent the time of last chondrule melting, whereas the ^{26}Al-^{26}Mg system reflects a secondary disturbance. In the second model (blue), we accept that the U-Pb and ^{26}Al-^{26}Mg systems both date the last chondrule melting event and the chondrule precursor is typified by a reduced initial $^{26}Al/^{27}Al$ inventory compared to the canonical abundance. The blue shaded area in Fig. 3 thus represents the range of values consistent with a subcanonical $^{26}Al/^{27}Al$ in the inner Solar System. In this case, the initial ^{26}Al abundance of the chondrule precursor ($[^{26}Al/^{27}Al]_0$) is back-calculated to the time of CAI formation from the observed $^{26}Al/^{27}Al$ value at the time of chondrule crystallization inferred from the Pb-Pb age. For both models, we assume that the measured bulk Al/Mg ratios of the chondrules represent that of their precursor material. Thus, this assumption requires that the chondrule formation mechanism does not modify the Al/Mg ratios of chondrules, which can occur, for example, by volatility controlled addition/removal of Mg to the chondrule melt. Olsen et al. (2016) reported the stable Mg isotope compositions ($\mu^{25}Mg$) and Al/Mg ratios of 42 individual chondriles from CV and CR chondrites. In detail, they show that the $\mu^{25}Mg$ variability is not correlated to the Al/Mg ratios of the chondrules, which is expected if the Al/Mg ratios are affected by evaporation/condensation of Mg. As such, these data do not provide evidence for Al/Mg fractionation during chondrule formation. Thus, we submit that the main assumption supporting our Mg evolution models is supported by existing data. For five chondrules, the intercept defined by the ^{26}Al-^{26}Mg isochrons, $\mu^{26}Mg^*_0$, and present-day bulk $\mu^{26}Mg^*$ values are not consistent within their stated uncertainties with the modeled radiogenic ingrowth predicted from a homogeneous distribution of ^{26}Al. In contrast, their ^{26}Al-^{26}Mg intercepts and present-day bulk $\mu^{26}Mg^*$ values are consistent with that inferred from a reduced $^{26}Al/^{27}Al$ ratio in the chondrule-forming reservoirs compared to the $[^{26}Al/^{27}Al]_0$ value in CAIs of $(5.252 \pm 0.019) \times 10^{-5}$ and corresponding $\mu^{26}Mg^*_0$ of -33.5 ppm. The ^{26}Al-^{26}Mg systematics of chondrules C3 and 5-C2 are consistent with both models whereas chondrule 5-C10 record a Mg isotope composition that appears to be intermediate between the two models. The reason for this observation is unclear but could reflect underestimation of the model uncertainties or, alternatively, partial disturbance of the ^{26}Al-^{26}Mg systematics. In summary, the $\mu^{26}Mg^*$ evolution of the majority of the chondrules studied here (5 out of 7) cannot be reconciled with the model of ^{26}Al homogeneity but are consistent with the proposal that the inner disk solids were characterized by a lower initial $^{26}Al/^{27}Al$ ratio relative to CAIs.

Having rejected the first three scenarios to explain the age mismatch between the Pb-Pb and ^{26}Al-^{26}Mg ages, namely (*i*) the uranium-corrected Pb-Pb ages are not accurate to their stated uncertainties, (*ii*) the Pb-Pb dates and Al-Mg ages reflect different events and/or processes and (*iii*) $^{238}U/^{235}U$ variability in chondrule precursors, we conclude that the most straightforward interpretation of the observed age mismatch is a reduced initial $^{26}Al/^{27}Al$ ratio in chondrule precursors. A reduced $^{26}Al/^{27}Al$ ratio amongst inner Solar System chondrules provides additional support to the idea that isotopically distinct disk reservoirs existed during the lifetime of the protoplanetary disk. Indeed, it has been suggested that a dichotomy exists in the nucleosynthetic composition of material that formed in the inner Solar System relative to material that accreted in the formation region of carbonaceous chondrites, which is hypothesized to be located within and beyond the orbits of the gas giants (Warren, 2011; van Kooten et al., 2016). Inner Solar System material typically records a depletion in the abundance of neutron-rich nuclides such as ^{54}Cr and ^{50}Ti relative to carbonaceous chondrites (i.e. Trinquier et al., 2009). Larsen et al. (2011) and Schiller et al. (2015a, 2015b) suggested that inner Solar System bodies such as the angrite parent body and ordinary chondrites are characterized by a reduced initial $^{26}Al/^{27}Al$ ratio of $\sim 1.5 \times 10^{-5}$ relative to the bulk Solar System value of $\sim 2.5 \times 10^{-5}$ defined by CI chondrites based on their Mg isotope compositions (Larsen et al., 2011). Thus, a distinct initial ^{26}Al abundance for the inner Solar System relative to carbonaceous chondrites is in line with the nucleosynthetic dichotomy that exists for numerous nucleosynthetic tracers (i.e. Trinquier et al., 2008, 2009; Paton et al.,2013; Schiller et al., 2015a, 2015b; Budde et al., 2016).

4.2. Origin of initial $^{26}Al/^{27}Al$ variability in chondrules

The initial $^{26}Al/^{27}Al$ values back-calculated to the time of CAI formation ($[^{26}Al/^{27}Al]_0$) recorded by the individual chondrules range from $(3.92^{-2.95}_{+4.53}) \times 10^{-6}$ to $(2.74^{-1.09}_{+1.30}) \times 10^{-5}$ (Table 2). In Fig. 4, we show that the range of values essentially defines two individual groups, which are apparently correlated to the absolute ages of the chondrules. The first group, which comprises four chondrules (2-C1, 5-C2, 5-C10, C30) that have absolute ages indistinguishable from CAIs, record an average $[^{26}Al/^{27}Al]_0$ corresponding to $(4.75^{-1.21}_{+1.99}) \times 10^{-6}$. The second group is defined by four

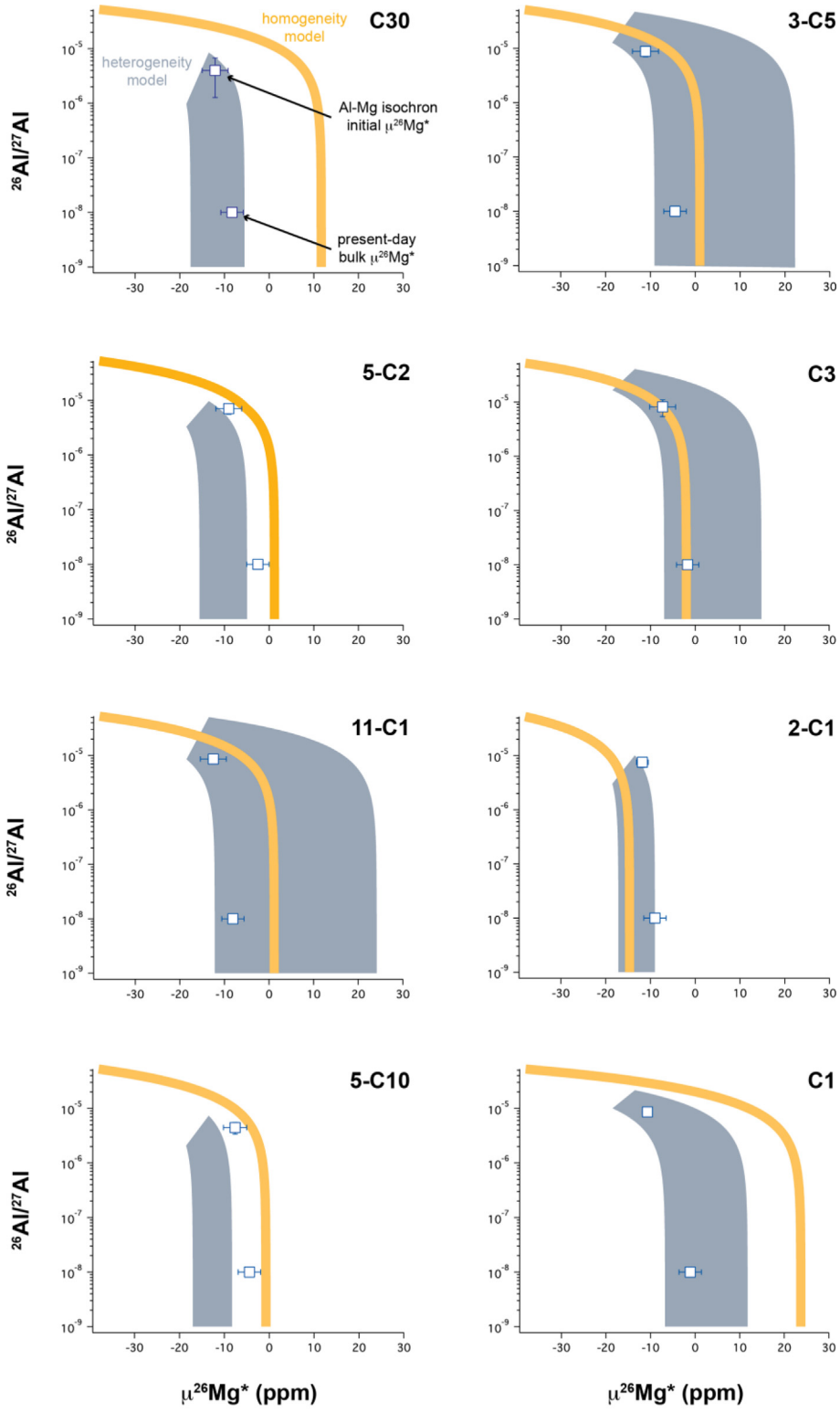

Fig. 3. $\mu^{26}Mg^*$ evolution diagrams for chondrules studied here relative to that predicted from models assuming heterogeneous (blue) and homogenous (yellow) ^{26}Al distribution. In the homogeneity model, the $[^{26}Al/^{27}Al]_0$ and initial $^{26}Mg/^{24}Mg$ ($\mu^{26}Mg_0$) isotope composition of the Solar System is taken to be $(5.252 \pm 0.019) \times 10^{-5}$ and -33.5 ppm, respectively (Jacobsen et al., 2008; Larsen et al., 2011). In the heterogeneity model, we assume that the chondrules' $[^{26}Al/^{27}Al]_0$ is that back-calculated to the time of CAI formation from the measured $^{26}Al/^{27}Al$ using the Pb-Pb ages of each chondrules. In this model, the initial $\mu^{26}Mg_0$ of the Solar System is from Larsen et al. (2011). All uncertainties associated with model parameters (i.e. absolute ages, $^{26}Al/^{27}Al$, $\mu^{26}Mg^*$ and $^{27}Al/^{24}Mg$ values) are propagated in final uncertainties. The shape and width of the blue area reflects the uncertainties associated with the heterogeneity model, which is dominated by the analytical uncertainties associated with the measurements.

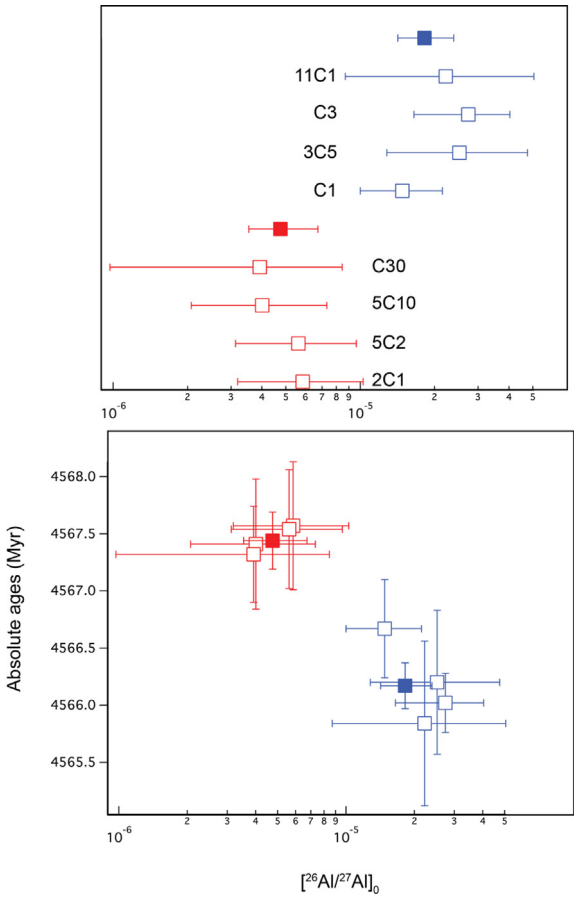

Fig. 4. Initial $^{26}Al/^{27}Al$ ratios ($[^{26}Al/^{27}Al]_0$) and absolute ages of chondrules studied here. The $[^{26}Al/^{27}Al]_0$ values are calculating by back-projecting the measured $^{26}Al/^{27}Al$ ratios to the time of CAI formation using the U-corrected Pb-Pb ages. Uncertainties on the Pb-Pb ages are propagated into the $[^{26}Al/^{27}Al]_0$ values. Solid symbols reflect weighted means and associated uncertainties.

chondrules that record ages that are approximately 1 Myr younger than CAIs (C1, 3-C5, C3, 11-C1), and define an average $[^{26}Al/^{27}Al]_0$ corresponding to $(1.82^{-0.40}_{+0.57}) \times 10^{-5}$. We explore below potential mechanisms to explain the apparent age dependency of the initial $^{26}Al/^{27}Al$ values of individual inner Solar System chondrules.

The nucleosynthetic isotopic variability for nuclides such as ^{54}Cr, ^{50}Ti and ^{48}Ca observed amongst Solar System's solids, asteroidal bodies and planets has been ascribed to variable thermal processing of the precursor material during the earliest stages of disk evolution (Trinquier et al., 2009). Thermal processing of molecular cloud material is hypothesized to cause the preferential loss by sublimation of thermally unstable and isotopically anomalous presolar carriers, producing residual isotopic heterogeneity. This hypothesis has been used explain the apparent dichotomy that exists in the nucleosynthetic composition of inner and outer Solar System bodies (i.e. Schiller et al., 2018). The material precursor to inner Solar System bodies has experienced high temperatures associated with the early mass accretion to the proto-Sun, resulting in efficient thermal processing and, hence, depletion in the relative abundances of nucleosynthetic tracers such as ^{54}Cr. In contrast, the bulk of the outer Solar System material was not thermally processed close to the proto-Sun and, therefore, record excesses in the abundance of the ^{54}Cr nucleosynthetic tracer relative to Earth. Larsen et al. (2011) noted that the variability in the inferred initial ^{26}Al abundance of bulk Solar System reservoirs resonate well with their $\mu^{54}Cr$ values. Reservoirs characterized by an increased initial abundance of ^{26}Al compared to the solar value defined by CI chondrites record excesses in ^{54}Cr whereas reservoirs typified by a sub-solar initial ^{26}Al abundance record ^{54}Cr deficits (Larsen et al., 2011; van Kooten et al., 2016). The Solar System's $^{26}Mg^*$-^{54}Cr correlation is interpreted as reflecting variable degrees of thermal processing of the precursor material, leading the preferential destruction of presolar carriers enriched in ^{26}Al and ^{54}Cr (Larsen et al., 2011; van Kooten et al., 2016). In this view, refractory inclusions [Ca-Al-rich inclusions (CAIs) and amoeboid olivine aggregates (AOAs)] represent samples of the complementary gaseous reservoir enriched in ^{26}Al by thermal processing, which resulted in the widespread ^{26}Al depletions observed among the inner Solar System bodies. Thus, a possibility is that the age dependency observed in the $[^{26}Al/^{27}Al]_0$ ratios of the chondrules reflect the different thermal histories of their precursor material. For example, the older chondrule population characterized by a low $[^{26}Al/^{27}Al]_0$ ratio may have formed from material that experienced more thermal processing relative to the younger chondrule population. However, the initial Pb isotope composition of the chondrules studied has been used to argue that the majority of chondrules formed within 1 Myr of Solar System formation and that these existing chondrules where recycled and remelted during the disk lifetime (Bollard et al., 2017). If this process occurred as a closed system, it is unlikely that younger chondrules would be characterized by a higher $[^{26}Al/^{27}Al]_0$ ratio relative to chondrules formed at early times.

It has been recently proposed that the nucleosynthetic variability observed amongst inner Solar System solids, asteroids and planets reflects the progressive admixing of pristine dust of CI composition to an initially thermally processed inner disk associated with the growth of the proto-Sun (Schiller et al., 2018). In this model, CI-like dust was available during the lifetime of the disk to fuel asteroidal and planetary growth. If chondrules formed at early times are indeed recycled and remolten during the disk lifetime, it seems unavoidable that this process will lead to the incorporation of fresh CI dust into chondrules during recycling. This prediction is consistent with the numerous observation of dust rims mantling chondrules in various chondrites (Leitner et al., 2016; Hanna and Ketcham, 2018). Moreover, Manhan et al. (2018) recently demonstrated the trace element budget of chondrules from the NWA 5697 ordinary chondrite is consistent with progressive admixing of volatile-rich CI dust during the disk lifetime. We show in Fig. 5a, the FeO/MnO ratio measured in olivine from NWA 5697, including the objects studied here, plotted against the chondrule absolute ages. The FeO/MnO ratio, which we use a proxy for volatility, shows

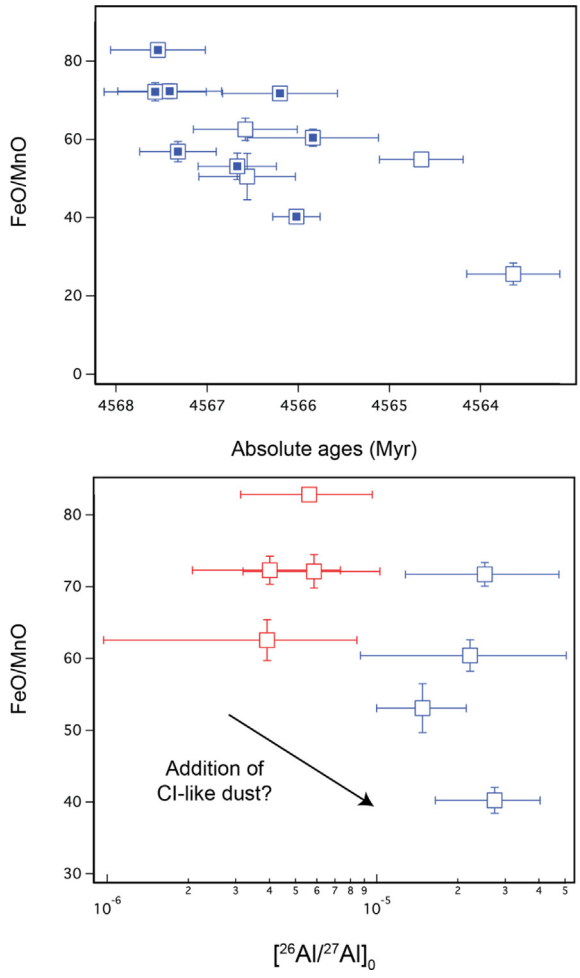

Fig. 5. Variation diagrams depicting the relationship between absolute ages, initial $^{26}Al/^{27}Al$ ($[^{26}Al/^{27}Al]_0$) and olivine FeO/MnO ratios of chondrules. The $[^{26}Al/^{27}Al]_0$ values are calculating by back-projecting the measured $^{26}Al/^{27}Al$ ratios to the time of CAI formation using the U-corrected Pb-Pb ages. Uncertainties on the Pb-Pb ages are propagated into the $[^{26}Al/^{27}Al]_0$ values. Solid symbols in upper panel reflect chondrules investigated here – the remainder of the chondrules are from NWA 5697. The FeO/MnO ratios are from Connelly et al. (2012) and Bollard et al. (2017). Blue symbols in lower panel are the young chondrule population whereas the red symbols depict the old population.

a clear progressive decrease with time, consistent with admixing of volatile-rich dust. Thus, admixing of CI dust, which has a higher initial abundance of ^{26}Al relative to thermally processed inner disk material (Larsen et al., 2011), is predicted to result in a higher $[^{26}Al/^{27}Al]_0$ ratio in younger chondrules relative to chondrules formed at early times. We show in Fig. 5b the $[^{26}Al/^{27}Al]_0$ ratios of chondrules studied here plotted against their FeO/MnO ratios. Although the data have large uncertainties, they are consistent with a decrease in the FeO/MnO ratio associated with a higher $[^{26}Al/^{27}Al]_0$. Thus, we conclude that the most straightforward interpretation of the observed age dependent variability of the chondrules' $[^{26}Al/^{27}Al]_0$ ratios is the admixing of ^{26}Al-rich CI dust during chondrule recycling. This requires that a decoupling existed between the volatile loss of Pb in chondrules and the sublimation of the carriers of the ^{26}Al and ^{54}Cr enrichments

4.3. Solid formation and accretion of inner disk protoplanets

The majority of chondrules from pristine unequilibrated ordinary chondrites record $^{26}Al/^{27}Al$ ratios at the time of crystallization ranging from $\sim 2 \times 10^{-5}$ to $\sim 8 \times 10^{-6}$, which corresponds to an age difference of ~1 to 2 Myr from the formation of CAIs (Huss et al., 2001; Mostefaoui et al., 2002; Rudraswami and Goswami, 2007; Villeneuve et al., 2009; Pape et al., 2019) assuming a uniform distribution of ^{26}Al at the start of the Solar System with a value of $\sim 5.2 \times 10^{-5}$ (Jacobsen et al., 2008; Larsen et al., 2011). This ~1 to 2 Myr age gap between the formation of CAIs and chondrules is similar to the mismatch between the ^{26}Al-^{26}Mg and Pb-Pb ages for the chondrules reported here. It is apparent that the so-called age-gap between the formation of CAIs and chondrules must predominately reflect a reduced $^{26}Al/^{27}Al$ ratio in chondrule precursors and, thus, has no chronological significance. In agreement with the absolute chronology of chondrule formation (Connelly et al., 2012; Bollard et al., 2017), we infer that the ^{26}Al-^{26}Mg data of chondrules from unequilibrated ordinary chondrites support the view that the formation of inner Solar System chondrules started contemporaneously with CAIs and lasted ~3 Myr. Recurrent chondrule formation during the lifetime of the solar protoplanetary disk implies that chondrules may represent the building blocks of differentiated asteroids and, by extension, protoplanetary bodies (Bollard et al., 2017). Lastly, our new data confirm the proposal that the ^{26}Al-^{26}Mg decay system does not provide an accurate chronology of disk processes assuming ^{26}Al homogeneity at a $^{26}Al/^{27}Al$ ratio of 5.25×10^{-5} (Larsen et al., 2011; Schiller et al., 2015a, 2015b; Bollard et al., 2017).

If chondrules are indeed the building blocks of asteroidal bodies in the inner Solar System, the ^{26}Al inventory of asteroids will be controlled by that of their precursor chondrules. Comparing the Pb-Pb and ^{26}Al-^{26}Mg ages of three angrites, Schiller et al. (2015a) observed an age mismatch of ~1.5 Myr between the absolute and relative ages, which they interpreted as reflecting a reduced $[^{26}Al/^{27}Al]_0$ ratio of the angrite parent body corresponding to $(1.33^{-0.18}_{+0.21}) \times 10^{-5}$. The angrite and ordinary chondrite parent bodies have identical ^{54}Cr compositions (Trinquier et al., 2007), suggesting that these two bodies formed from similar precursor material. Reassuringly, the average $[^{26}Al/^{27}Al]_0$ ratio recorded by our eight chondrules corresponds to $(1.36 \pm 0.72) \times 10^{-5}$, which is identical within uncertainty to that inferred for the angrite parent body. Moreover, based on the $\mu^{26}Mg^*$ value of ordinary chondrites, Larsen et al. (2011) inferred an $[^{26}Al/^{27}Al]_0$ ratio of $(1.63 \pm 0.25) \times 10^{-5}$ for this parent body, which is identical to our independent estimate based on chondrules. Such striking consistency provides strong support for the accuracy of our data and model.

During the initial stages of planet formation, dust grains collide to form asteroidal bodies, which represent the kilometer-sized building blocks of protoplanets (Johansen

et al., 2015). The diversity of igneous meteorites suggests that widespread silicate melting and differentiation of rocky bodies occurred within the first few million years of the Solar System (Bizzarro et al. 2005; McCoy et al., 2006; Schiller et al., 2011, 2015a; Kruijer et al., 2014; Larsen et al. 2016b). The energy released from the decay of the ^{26}Al nuclide is believed to be the main heat source driving asteroidal melting (Bizzarro et al., 2005; Hevey and Sanders, 2006) requiring that the accretion of differentiated asteroids occurred within the life span of ^{26}Al. As such, a reduced initial ^{26}Al/^{27}Al ratio in the precursor material of inner Solar System planetary objects impacts our understanding of the accretion timescales of differentiated asteroids. For an ordinary chondrite type source rock, the onset of silicate melting is defined by the silicate solidus temperature of 1350 K (McCoy et al., 2006), and approximately 50% partial melting (1650 K) is required to generate asteroid-wide magma oceans and, thus, full differentiation (Moskovitz and Gaidos, 2011).

We show in Fig. 6 the minimum $[^{26}Al/^{27}Al]_0$ ratio required to achieve up to 50% melting as inferred from our thermal models, with respect to the accretion timescales from CAI formation. We observe that both melting curves intercept our chondrule precursor $[^{26}Al/^{27}Al]_0$ ratios,

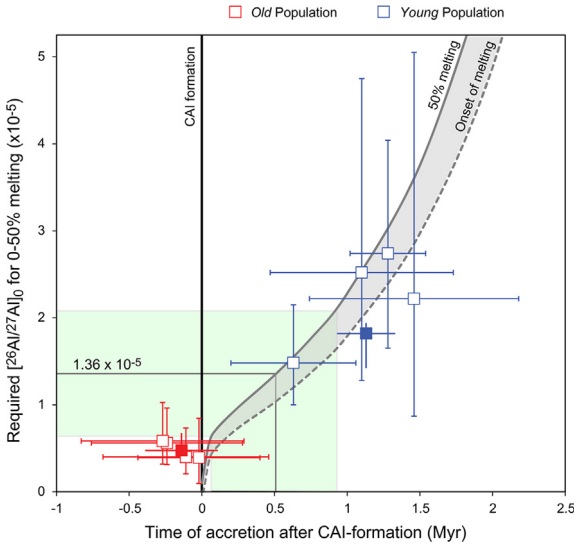

Fig. 6. Thermal evolution models. The results of thermal models showing the minimum initial (^{26}Al/^{27}Al) ($[^{26}Al/^{27}Al]_0$) required to achieve 0–50% melting in an ordinary chondrite type of source rock for large asteroids (100 km in radius). Dashed grey line represents the onset of silicate melting (1350 K) in asteroids interior as a function of accretion time, whereas solid gray line represents 50% melting (1650 K) required to fully differentiate the asteroid. Vertical line represents the time of CAI-formation at 4567.30 ± 0.16 Myr (Connelly et al., 2012). Squares represent the precursor initial $[^{26}Al/^{27}Al]_0$ calculated for each chondrule. Solid symbols represent weighted average initial $[^{26}Al/^{27}Al]_0$ of old and young chondrule populations. The grey area represents the initial $[^{26}Al/^{27}Al]_0$ that only permits partial melting of the asteroid. The green band represent the average $[^{26}Al/^{27}Al]_0$ inferred from the chondrules and the timing of accretion required for melting with this initial value.

thereby showing that it is possible to partially melt planetesimals that accreted as early as the CAI-formation period from material with such a reduced initial ^{26}Al/^{27}Al ratio. We note that that a minimum disk temperature of ~500 K is required to achieve partial melting in a planetesimal that accretes within the 100,000 years after CAI formation. This is consistent with the recent study of Larsen et al. (2016b) who interpreted the negative μ^{26}Mg* compositions characterizing the Main Group and pyroxene pallasites and primitive achondrites as accretion from material depleted in ^{26}Al, within 250,000 years of Solar System formation in a hot (>500 K) protoplanetary disk. Moreover, Schiller et al. (2015a) inferred a similar accretion timescale of $0.25^{-0.19}_{+0.17}$ Myr relative to CAI-formation for the angrite parent body from the calculated reduced $[^{26}Al/^{27}Al]_0$ value. We further note that, even though the disk temperature decreases with time, the increase in $[^{26}Al/^{27}Al]_0$ observed in younger chondrules will provide enough energy from ^{26}Al decay to keep partially melting the outer layers of the planetesimal, until at least 1 Myr post-CAIs. Continuous accretion onto this planetesimal after 1 Myr and throughout the disk lifetime results in an unmelted chondritic capping on top of the melted interior (Weiss and Elkins-Tanton, 2013; Larsen et al., 2016b). Inner Solar System chondrules with Pb-Pb ages up to about 4 Myr older than CAIs (Connelly et al., 2012; Bollard et al., 2017) provide the source material for such continuous planetesimal accretion. Using the average $[^{26}Al/^{27}Al]_0$ value of $(1.36 \pm 0.72) \times 10^{-5}$ for the eight chondrules requires accretion within ~0.1 to ~0.9 Myr after Solar System formation to ensure 50% melting by ^{26}Al decay for bodies that formed with this initial ^{26}Al content. These results support the idea that the initial stage of planet formation, namely the accretion of micrometer-sized dust into bodies of 1–1000 km that can undergo run-away accretion, is a rapid and efficient process (Johansen et al., 2015). Differentiated meteorites are thought to represent fragments of asteroids that accreted early when the abundance of ^{26}Al was high enough to induce asteroid-wide melting whereas chondritic meteorites represent samples of late forming asteroids (Bizzarro et al., 2005). However, accepting that accretion is a rapid and efficient processes as indicated by our results, it is unclear how it can be delayed in the region(s) where chondritic parent bodies formed. A possibility is that chondrites do not represent samples of late accreting asteroids but rather late accreting crustal layers of material onto existing early-accreted differentiated planetesimal seeds (Elkins-Tanton et al., 2011; Weiss and Elkins-Tanton, 2013; Larsen et al., 2016b). In this scenario, based on the observation of chondrule formation over a period of ~4 Myr (Connelly et al., 2012; Bollard et al., 2017), accretion is a continuous process during the early evolution of the protoplanetary disk and chondrites represent samples of the late-accreted outer unmelted shells of differentiated planetesimals with silicate mantles and metallic cores. If correct, these results and interpretations support the idea that partially differentiated asteroids are common in the asteroid belt and that chondrules played a significant role in their formation.

5. CONCLUSIONS

We have conducted, for the first time, an in-situ SIMS and high-precision bulk analysis of the Mg and the ^{54}Cr isotopic composition of eight individual chondrules previously dated by the U-corrected Pb-Pb method. The resulting ^{26}Al-^{26}Mg isochrons yielded younger ages ranging between ~0.7–2.7 Myr relative to the corresponding U-corrected absolute Pb-Pb ages. This offset between the Al-Mg and Pb-Pb ages is interpreted to reflect a reduced initial ^{26}Al/^{27}Al ratio in the chondrule precursor material relative to the so-called canonical value defined by CAIs. Coupling our Al-Mg data with the absolute U-corrected Pb-Pb ages allowed us to constrain the initial ^{26}Al abundance in the chondrule precursor material at the time of CAI formation. All chondrules record subcanonical $[^{26}Al/^{27}Al]_0$ ratios ranging from $(3.92^{-2.95}_{+4.53}) \times 10^{-6}$ to $(2.74^{-1.09}_{+1.30}) \times 10^{-5}$. In fact, our data define two chondrule populations: an old population with Pb-Pb ages identical to CAIs that yields a weighted mean $[^{26}Al/^{27}Al]_0$ ratio of $(4.75^{-1.21}_{+1.99}) \times 10^{-6}$ that is ~11 times lower than the canonical value and a young population (~1 Myr) with a weighted mean $[^{26}Al/^{27}Al]_0$ ratio of $(1.82^{-0.40}_{+0.57}) \times 10^{-5}$ that is ~3 times lower than the canonical value.

All chondrules record ^{54}Cr compositions consistent with their formation in the inner Solar System. Consequently, we interpret the reduced $[^{26}Al/^{27}Al]_0$ ratios recorded by the chondrules relative to the canonical value as reflecting their formation from thermally-processed and ^{26}Al-depleted inner disk material. In the context of recent models of primary dust origin and processing (Trinquier et al., 2009; Paton et al., 2013; Bizzarro et al., 2017), the observed variability in the $[^{26}Al/^{27}Al]_0$ as resulting from unmixing by thermal processing of presolar dust components that was physically well-mixed but heterogeneous in composition at the grain scale. In this model, a new supernova dust component enriched in ^{26}Al and thermally unstable is preferentially sublimated relative to an older galactic background dust component, depleted in ^{26}Al. The chondrules represent samples of the residual thermally processed ^{26}Al depleted disk material. Moreover, we propose that the observed age dependent variability of the chondrules' $[^{26}Al/^{27}Al]_0$ ratio is the admixing of ^{26}Al-rich CI dust during chondrule recycling. The average $[^{26}Al/^{27}Al]_0$ of the eight chondrules corresponds to $(1.36 \pm 0.72) \times 10^{-5}$, which is identical to the $[^{26}Al/^{27}Al]_0$ ratio of $(1.33^{-0.18}_{+0.21}) \times 10^{-5}$ defined for the angrite parent body (Schiller et al., 2015a, 2015b).

Our data and interpretation indicate that the bulk of the material which accreted to form the ^{54}Cr-poor primitive and differentiated asteroids and, by extension, the protoplanets of the inner Solar System, had an $[^{26}Al/^{27}Al]_0$ ratio of $\sim 1.5 \times 10^{-5}$ at the time of Solar System formation. This has two major consequences for understanding the early dynamic of the protoplanetary disk. First, this spatial and temporal variability in ^{26}Al abundance rules out a general chronological significance of ^{26}Al-^{26}Mg system for unrelated objects. Second, considering the decay of the ^{26}Al radionuclide as the main heat source to achieve melting in asteroids, this reduced initial ^{26}Al/^{27}Al ratio amongst inner Soalr System objects constrains the timing of asteroids melting and differentiation. With a thermal evolution model of a 100 km in radius asteroid, we show that melting can occur, in a hot protoplanetary disk with an initial $[^{26}Al/^{27}Al]_0$ ratio as low as $\sim 4.75 \times 10^{-6}$, if accretion occurs as early as 10,000 to 100,000 years after the formation of CAIs from a hot (>500 K) inner protoplanetary disk. Over the first million years of evolution, while the inner disk regions cool, melting may still occur when the higher ^{26}Al budget recorded in younger chondrules is accreted to planetesimals. After ~1.0–1.5 Myr, further accretion will lead to the formation of an undifferentiated shell on top of differentiated material and may represent the source of chondrite meteorites.

ACKNOWLEDGEMENTS

Funding for this project was provided by grants from the Danish National Research Foundation (grant number DNRF97) and from the European Research Council (ERC Consolidator grant agreement 616027-STARDUST2ASTEROIDS) to M.B. and from Kakenhi Monkasho to H.Y. We thank Andrew Davis, Marc Chassidon, Tim Gregory and Associate Editor Sara Russell for their constructive review of our paper, which resulted in significantly improving the quality of our work.

APPENDIX A. SUPPLEMENTARY MATERIAL

Supplementary data to this article can be found online at https://doi.org/10.1016/j.gca.2019.06.025.

REFERENCES

Amelin Y. (2008) U-Pb ages of angrites. *Geochim. Cosmochim. Acta* **72**, 221–232.

Amelin Y., Kaltenbach A., Iizuka T., Stirling C. H., Ireland T. R., Petaev M. and Jacobsen S. B. (2010) U-Pb chronology of the Solar System's oldest solids with variable ^{238}U/^{235}U. *Earth Planet. Sci. Lett.* **300**, 343–350.

Bizzarro M., Baker J. A., Haack H. and Lundgaard K. L. (2005) Rapid timescales for accretion and melting of differentiated planetesimals inferred from ^{26}Al-^{26}Mg chronometry. *Astrophys. J.* **632**, L41–L44.

Bizzarro M., Paton C., Larsen K. K., Schiller M., Trinquier A. and Ulfbeck D. (2011) High-precision Mg-isotope measurements of terrestrial and extraterrestrial material by HR-MC-ICPMS - implications for the relative and absolute Mg-isotope composition of the bulk silicate Earth. *J. Anal. At. Spectrom.* **26**, 565–577.

Bizzarro M., Connelly J. N. and Krot A. N. (2017) Chondrules: ubiquitous chondritic solids tracking the evolution of the solar protoplanetary disk. In *Formation, Evolution, and Dynamics of Young Solar Systems. Astrophysics and Space Science Library* (eds. M. Pessah and O. Gressel). Springer, Cham, pp. 161–195.

Bollard J., Connelly J. N. and Bizzarro M. (2015) Pb-Pb dating of individual chondrules from the CBa chondrite Gujba: Assessment of the impact plume formation model. *Meteorit. Planet. Sci.* **50**, 1197–1216.

Bollard J., Connelly J. N., Whitehouse M. J., Pringle E. A., Bonal L., Jørgensen J. K., Nordlund Å., Moynier F. and Bizzarro M. (2017) Early formation of planetary building blocks inferred from Pb isotopic ages of chondrules. *Sci. Adv.* **3**, e1700407.

Boss A. P. and Ciesla F. J. (2014) Short-lived radionuclides and early solar system chronology. In *Planets, Asteroids, Comets and the Solar SystemTreatise on Geochemistry, 2nd ed. (Exec. Eds. H. D. Holland and K. K. Turekian)*, vol. 2 (ed. A. M. Davis). Elsevier, Oxford, pp. 37–53.

Brennecka G., Weyer S., Wadhwa M., Janney P., Zipfel J. and Anbar A. (2010) $^{238}U/^{235}U$ variations in meteorites: extant ^{247}Cm and implications for Pb–Pb dating. *Science* **327**, 449–451.

Budde G., Burkhardt C., Brennecka G. A., Fischer-Gödde M., Kruijer T. S. and Kleine T. (2016) Molybdenum isotopic evidence for the origin of chondrules and a distinct genetic heritage of carbonaceous and non-carbonaceous meteorites. *Earth Planet. Sci. Lett.* **454**, 293–303.

Castillo-Rogez J., Johnson T. V., Lee M. H., Matson D. L. and Lunine J. (2009) ^{26}Al decay: Heat production and a revised age for Iapetus. *Icarus* **204**, 658–662.

Chaussidon M., Libourel G. and Krot A. N. (2008) Oxygen isotopic constraints on the origin of magnesian chondrules and on the gaseous reservoirs in the early Solar System. *Geochim. Cosmochim. Acta* **72**, 1924–1938.

Connelly J. N., Bizzarro M., Thrane K. and Baker J. A. (2008) The Pb-Pb age of angrite SAH 99555 revisited. *Geochim. Cosmochim. Acta* **72**, 4813–4824.

Connelly J. N., Bizzarro M., Krot A. N., Nordlund Å., Wielandt D. and Ivanova M. A. (2012) The absolute chronology and thermal processing of solids in the solar protoplanetary disk. *Science* **338**, 651–655.

Connelly J. N., Bollard J. and Bizzarro M. (2017) Pb-Pb chronometry and the early Solar System. *Geochim. Cosmochim. Acta* **201**, 345–363.

Connelly J. N. and Bizzarro M. (2018) The absolute Pb–Pb isotope ages of chondrules. In *Chondrules: Records of Protoplanetary Disk Processes (Cambridge Planetary Science* (eds. S. Russell, H. Connolly and A. Krot). Cambridge University Press, Cambridge, pp. 300–323.

Connelly J. N. and Bizzarro M. (2009) Step leaching Pb-Pb ages of chondrules from chondrites Allende. *Chem. Geol.* **72**, 4813–4824.

Connelly J. N. and Bizzarro M. (2016) Lead isotope evidence for a young formation age of the Earth-Moon system. *Earth Planet. Sci. Lett.* **452**, 36–43.

Elkins-Tanton L. T., Weiss B. P. and Zuber M. T. (2011) Chondrites as samples of differentiated planetesimals. *Earth Planet. Sci. Lett.* **305**, 1–10.

Girault F., Perrier F., Moreira M., Zanda B., Rochette P. and Teitler Y. (2017) Effective radium-226 concentration in meteorites. *Geochim. Cosmochim. Acta* **208**, 198–219.

Gaidos E., Krot A. N., Williams J. P. and Raymond S. N. (2009) ^{26}Al and the Formation of the Solar System from a Molecular Cloud Contaminated by Wolf-Rayet Winds. *Astrophys. J.* **696**, 1854–1863.

Garver E. and Baskaran M. (2004) Effects of heating on the emanation rates of radon-222 from a suite of natural minerals. *Appl. Radiat. Isot.* **61**, 1477–1485.

Hanna R. D. and Ketcham R. A. (2018) Evidence for accretion of fine-grained rims in a turbulent nebula for CM Murchison. *Earth Planet. Sci. Lett.* **481**, 201–211.

Hevey P. J. and Sanders I. S. (2006) A model for planetesimal meltdown by ^{26}Al and its implications for meteorite parent bodies. *Meteorit. Planet. Sci.* **41**, 95–106.

Holst J. C., Olsen M. B., Paton C., Nagashima K., Schiller M., Wielandt D., Larsen K. K., Connelly J. N., Jørgensen J. K., Krot A. N., Nordlund A. and Bizzarro M. (2013) ^{182}Hf-^{182}W age dating of a ^{26}Al-poor inclusion and implications for the origin of short-lived radioisotopes in the early Solar System. *Proc. Natl. Acad. Sci.* **110**, 8819–8823.

Huss G. R., MacPherson G. J., Wasserburg G. J., Russell S. S. and Srinivasan G. (2001) Aluminum-26 in calcium-aluminum-rich in inclusions and chondrules from unequilibrated ordinary chondrites. *Meteorit. Planet. Sci.* **36**, 975–997.

Hutcheon I. D., Marhas K. K., Krot A. N., Goswami J. N. and Jones R. H. (2009) ^{26}Al in plagioclase-rich chondrules in carbonaceous chondrites: Evidence for an extended duration of chondrule formation. *Geochim. Cosmochim. Acta* **73**, 5080–5099.

Hutchison R. (2004) *Meteorites: A Petrologic, Chemical and Isotopic Synthesis*. Cambridge University Press.

Ishimori Y., Lange K., Martin Y. S. and Phaneuf M. (2013) Measurement and calculation of radon releases from NORM residues. *Int. Atom. Energy Agency Tech. Rep. Ser.* **474**, 85.

Itoh S., Makide K. and Yurimoto H. (2008) Calculation of radiogenic ^{26}Mg of CAI minerals under high precision isotope measurement by SIMS. *Appl. Surf. Sci.* **255**, 1476–1478.

Jacobsen B., Yin Q.-Z., Moynier F., Amelin Y., Krot A. N., Nagashima K., Hutcheon I. D. and Palme H. (2008) ^{26}Al-^{26}Mg and ^{207}Pb-^{206}Pb systematics of Allende CAIs: Canonical solar initial $^{26}Al/^{27}Al$ ratio reinstated. *Earth Planet. Sci. Lett.* **272**, 353–364.

Johansen A., Mac Low M.-M., Lacerda P. and Bizzarro M. (2015) Growth of asteroids, planetary embryos, and Kuiper belt objects by chondrule accretion. *Sci. Adv.* **1**, e1500109.

Jones R. H. (1990) Petrology and mineralogy of Type II, FeO-rich chondrules in Semarkona (LL3.0): Origin by closed-system fractional crystallization, with evidence for supercooling. *Geochim. Cosmochim. Acta* **54**, 1785–1802.

Kawasaki N., Kato C., Itoh S., Wakaki S., Ito M. and Yurimoto H. (2015) ^{26}Al–^{26}Mg chronology and oxygen distributions of multiple melting for a Type C CAI from Allende. *Geochim. Cosmochim. Acta* **169**, 99–114.

Kawasaki N., Itoh S., Sakamoto N. and Yurimoto H. (2017) Chronological study of oxygen isotope composition for the solar protoplanetary disk recorded in a fluffy Type A CAI from Vigarano. *Geochim. Cosmochim. Acta* **201**, 83–102.

Kawasaki N., Simon S. B., Grossman L., Sakamoto N. and Yurimoto H. (2018) Crystal growth and disequilibrium distribution of oxygen isotopes in an igneous Ca-Al-rich inclusion from the Allende carbonaceous chondrite. *Geochim. Cosmochim. Acta* **221**, 318–341.

Kimura M., Nakajima H., Hiyagon H. and Weisberg M. K. (2006) Spinel group minerals in LL3.00-6 chondrites: Indicators of nebular and parent body processes. *Geochim. Cosmochim. Acta* **70**, 5634–5650.

Kita K. T., Nagahara H., Togashi S. and Morishita Y. (2010) A short duration of chondrule formation in the solar nebula: Evidence from ^{26}Al in Semarkona ferromagnesian chondrules. *Geochim. Cosmochim. Acta* **64**, 3913–3922.

Krot A. N., Amelin Y., Cassen P. and Meibom A. (2005) Young chondrules in CB chondrites from a giant impact in the early Solar System. *Nature* **436**, 989–992.

Krot A. N., Amelin Y., Bland P., Ciesla F. J., Connelly J., Davis A. M., Huss G. R., Hutcheon I. D., Makide K., Nagashima K., Nyquist L. E., Russell S. S., Scott E. R. D., Thrane K., Yurimoto H. and Yin Q.-Z. (2009) Origin and chronology of chondritic components: A review. *Geochim. Cosmochim. Acta* **73**, 4963–4997.

Kruijer T. S., Touboul M., Fischer-Godde M., Bermingham K. R., Walker R. J. and Kleine T. (2014) Protracted core formation and rapid accretion of protoplanets. *Science* **344**, 1150–1154.

La Tourette T. and Wasserburg G. J. (1998) Mg diffusion in anorthite: implications for the formation of early solar system planetesimals. *Earth Planet. Sci. Lett.* **158**, 91–108.

Larsen K. K., Trinquier A., Paton C., Schiller M., Wielandt D., Ivanova M. A., Connelly J. N., Nordlund Å., Krot A. N. and Bizzarro M. (2011) Evidence for magnesium isotope heterogeneity in the solar protoplanetary disk. *Astrophys. J.* **735**, L37.

Larsen K. K., Wielandt D., Schiller M. and Bizzarro M. (2016a) Chromatographic speciation of Cr(III)-species, inter-species equilibrium isotope fractionation and improved chemical purification strategies for high-precision isotope analysis. *J. Chromatogr. A* **1443**, 162–174.

Larsen K. K., Schiller M. and Bizzarro M. (2016b) Accretion timescales and style of asteroidal differentiation in an ^{26}Al-poor protoplanetary disk. *Geochim. Cosmochim. Acta* **176**, 295–315.

Lee T., Papanastassiou D. A. and Wasserburg G. J. (1976) WasserburgDemonstration of 26Mg excess in Allende and evidence for ^{26}Al. *Geophys. Res. Lett.* **3**, 109–112.

Leitner J., Vollmer C., Floss C., Zipfel J. and Hoppe P. (2016) Ancient stardust in fine-grained chondrule dust rims from carbonaceous chondrites. *Earth Planet. Sci. Lett.* **434**, 117–128.

Lodders K. and Fegley, Jr., B. (1998) *The Planetary Scientist's Companion*. Oxford University Press, pp. 1–392.

Makide K., Nagashima K., Krot A. N., Huss G. R., Ciesla F. J., Hellebrand E., Gaidos E. and Yang L. (2011) Heterogenous distribution of ^{26}Al at the birth of the Solar System. *Astrophys. J.* **733**, L31.

Manhan B., Moynier F., Siebert J., Gueguen B., Agranier A., Pringle E. A., Bollard J., Connelly J. N. and Bizzarro M. (2018) Volatile element evolution of chondrules through time. *Proc. Natl. Acad. Sci.* **115**, 8547–8552.

Mare E. R., Tomkins A. G. and Godel B. M. (2014) Restriction of parent body heating by metal-troilite melting: Thermal models for the ordinary chondrites. *Meteorit. Planet. Sci.* **49**, 636–651.

McCoy T. J., Mittlefehldt D. W. and Wilson L. (2006) Asteroid differentiation. In *Meteorites and the Early Solar System II* (eds. D. Lauretta, H. Y. McSween, D. Lauretta and H. Y. McSween). Univ. of Arizona Press, pp. 733–745.

Moskovitz N. and Gaidos E. (2011) Differentiation of planetesimals and the thermal consequences of melt migrations in the early Solar System. *Meteorit. Planet. Sci.* **46**, 903–918.

Mostefaoui S., Kita N. T., Togashi S., Tachibana S., Nagahara H. and Morishita Y. (2002) The relative formation ages of ferromagnesian chondrules inferred from their initial aluminum-26/aluminum-27ratios. *Meteorit. Planet. Sci.* **37**, 421–438.

Nyquist L. E., Kleine T., Shih C. Y. and Reese Y. D. (2009) The distribution of short-lived radioisotopes in the early solar system and the chronology of asteroid accretion, differentiation, and secondary mineralization. *Geochim. Cosmochim. Acta* **73**, 5115–5136.

Olsen M. B., Wielandt D., Schiller M., Van Kooten E. M. M. E. and Bizzarro M. (2016) Magnesium and ^{54}Cr isotope compositions of carbonaceous chondrite chondrules – Insights into early disk processes. *Geochim. Cosmochim. Acta* **191**, 118–138.

Ouelette N., Desch S., Bizzarro M., Boss A. P., Ciesla F. and Meyer B. (2009) Injection mechanisms of short-lived nuclides and their homogenization. *Geochim. Cosmochim. Acta* **73**, 4946–4962.

Paton C., Hellstrom J., Paul B., Woodhead J. and Hergt J. (2011) Iolite: Freeware for the visualization and processing of mass spectrometric data. *J. Anal. At. Spectrom.* **26**, 2508–2518.

Paton C., Schiller M. and Bizzarro M. (2013) Identification of an ^{84}Sr-depleted carrier in primitive meteorites and implications for thermal processing in the solar protoplanetary disk. *Astrophys. J.* **763**, L40.

Pape J., Mezger K., Bouvier A.-S. and Baumgartner L. P. (2019) Time and duration of chondrule formation: Constraints from ^{26}Al-^{26}Mg ages of individual chondrules. *Geochim. Cosmochim. Acta* **244**, 416–436.

Rambaldi E. R. and Wasson J. T. (1981) Metal and associated phases in Bishunpur, a highly unequilibrated ordinary chondrite. *Geochim. Cosmochim. Acta* **45**, 1001–1015.

Rudraswami N. G. and Goswami J. N. (2007) 26Al in chondrules from unequilibrated L chondrites: Onset and duration of chondrule formation in the early solar system. *Earth Planet. Sci. Lett.* **257**, 231–244.

Schiller M., Baker J. A., Creech J., Paton C., Millet M. A., Irving A. and Bizzarro M. (2011) Rapid timescale for magma ocean crystallisation on the howardite-eucrite-diogenite parent body. *Astrophys. J.* **740**, L22.

Schiller M., Van Kooten E. M. M. E., Holst J. C., Olsen M. B. and Bizzarro M. (2014) Precise measurement of chromium isotopes by MC-ICPMS. *J. Anal. At. Spectrom.* **29**, 1406–1416.

Schiller M., Connelly J. N., Glad A., Mikouchi T. and Bizzarro M. (2015a) Early accretion of protoplanets inferred from a reduced inner Solar System ^{26}Al inventory. *Earth Planet. Sci. Lett.* **15**, 45–54.

Schiller M., Paton C. and Bizzarro M. (2015b) Evidence for nucleosynthetic enrichment of the protosolar molecular cloud core by multiple supernova events. *Geochim. Cosmochim. Acta* **149**, 88–102.

Schiller M., Bizzarro M. and Fernandes V. A. (2018) Isotopic evolution of the protoplanetary disk and the building blocks of Earth and the Moon. *Nature* **555**, 501–510.

Scott E. R. D. (2007) Chondrites and the protoplanetary disk. *Annu. Rev. Earth Planet. Sci.* **35**, 577–620.

Thrane K., Nagashima K., Krot A. N. and Bizzarro M. (2008) Discovery of a new FUN CAI from a CV carbonaceous chondrite: Evidence for multistage thermal processing in the protoplanetary disk. *Astrophys. J.* **680**, L141.

Trinquier A., Birck J.-L. and Allègre C. (2007) Widespread ^{54}Cr heterogeneity in the inner Solar System. *Astrophys. J.* **655**, 1179–1185.

Trinquier A., Birck J.-L. and Allègre C. J. (2008) High-precision analysis of chromium isotopes in terrestrial and meteorite samples by thermal ionization mass spectrometry. *J. Anal. At. Spectrom.* **23**, 1565–1574.

Trinquier A., Elliott T., Ulfbeck D., Coath C., Krot A. N. and Bizzarro M. (2009) Origin of nucleosynthetic isotope heterogeneity in the solar protoplanetary disk. *Science* **324**, 374–376.

Urey H. C. (1955) The cosmic abundances of potassium, uranium, and thorium and the heat balances of the Earth, the Moon, and Mars. *PNAS* **41**, 127–144.

Vasileiadis A., Nordlund Å. and Bizzarro M. (2013) Abundance of ^{26}Al and ^{60}Fe in evolving giant molecular clouds. *Astrophys. J. Lett.* **769**, L8.

Villeneuve J., Chaussidon M. and Libourel G. (2009) Homogeneous distribution of ^{26}Al in the Solar System from the Mg isotopic composition of chondrules. *Science* **325**, 985–988.

Van Kooten E. M. M., Wielandt D., Schiller M., Nagashima K., Thomen A., Larsen K. K., Olsen M. B., Nordlund Å., Krot A. N. and Bizzarro M. (2016) Isotopic evidence for primordial molecular cloud material in metal-rich carbonaceous chondrites. *Proc. Natl. Acad. Sci.* **113**, 2011–2016.

Warren P. H. (2011) Stable-isotopic anomalies and the accretionary assemblage of the Earth and Mars: a subordinate role for carbonaceous chondrites. *Earth Planet. Sci. Lett.* **311**, 93–100.

Weiss B. P. and Elkins-Tanton L. T. (2013) Differentiated planetesimals and the parent bodies of chondrites. *Annu. Rev. Earth Planet. Sci.* **41**, 529–560.

Young E. D. and Galy A. (2004) The isotope geochemistry and cosmochemistry of magnesium. *Rev. Mineral. Geochem.* **55**, 197–230.

Yurimoto H., Abe K.-I., Abe M., Ebihara M., Fujimura A., Hashiguchi M., Hashizume K., Ireland T. R., Itoh S., Katayama J., Kato C., Kawaguchi J., Kawasaki N., Kitajima F., Kobayashi S., Meike T., Mukai T., Nagao K., Nakamura T., Naraoka H., Noguchi T., Okazaki R., Park C., Sakamoto N., Seto Y., Takei M., Tsuchiyama A., Uesugi M., Wakaki S., Yada, Yamamoto K., Yoshikawa M. and Zolensky M. E. (2011) Oxygen isotopic compositions of asteroidal materials returned from Itokawa by the Hayabusa mission. *Science* **333**, 1116–1119.

Zanda B. (2004) Chondrules. *Earth Planet. Sci. Lett.* **224**, 1–17.

Associate editor: Sara S. Russell